Journal of Structural Geology, Vol. 11, No. 4, pp. 473 to 492, 1989
Printed in Great Britain

0191-8141/89 $03.00 + 0.00

The last 25 Ma of rotational deformation in part of the New Zealand plate-boundary zone

S. H. LAMB

Department of Earth Sciences, Bullard Laboratories, Madingley Road, Cambridge CB3 0ZE, U.K.

and

H. M. BIBBY

Geophysics Division, Department of Industrial and Scientific Research, Wellington, New Zealand

(*Received* 30 *March* 1988; *accepted in revised form* 25 *October* 1988)

Abstract—The Marlborough fault system is a zone of dextral transpression in continental crust, and marks the southern end of the Hikurangi subduction system between the obliquely convergent Australian and Pacific plates. Detailed mapping over an area of 100 km^2 has revealed a complex history of deformation during the last 25 Ma. The development of a thrust belt in the Miocene, referred to as D_1 deformation, was synchronous with the deposition of a thick submarine fan complex. The beginning of D_1 deformation may mark the initiation of the subduction zone in this part of the plate-boundary zone. Subsequently, in the Plio-Pleistocene, the region formed a zone of dextral shear, marked by major strike-slip faults and zones of distributed deformation, referred to as D_2 deformation. Crustal blocks, less than 5 km across, may have rotated *ca* 60° clockwise about vertical axes relative to the Pacific plate in the last 4 Ma. The pattern of deformation during the last 10 Ka to 100 years is consistent with the long-term D_2 deformation, and suggests that large crustal blocks resting on the subducted Pacific plate have rotated clockwise about vertical axes relative to the Pacific plate, accommodated by dextral shear further to the SW in the Marlborough fault system. The overall effect of the deformation has been the rotation of the edge of the southern part of the Hikurangi margin from a W to NW trend in the early Miocene to a NE trend today.

INTRODUCTION

MANY active and convergent plate-boundary zones have a significant component of relative plate motion parallel to the length of the plate-boundary zone (Woodcock 1986). Distributed deformation within the plate-boundary zone, which accommodates the relative plate motion, will be rotational with a component of horizontal simple shear. However, recognizing this in fossil orogenic belts is a major problem in structural geology.

New Zealand plate-boundary zone

The New Zealand plate-boundary zone between the Pacific and Australian plates provides a good opportunity to study rotational deformation with a large component of horizontal simple shear (Fig. 1). The instantaneous and long-term (>3 Ma) plate motions, as well as the short-term (>100 Ka) deformation styles and rates are well studied. In the northern part of the New Zealand plate-boundary zone, the Pacific plate is being obliquely subducted beneath the Australian plate along the Hikurangi margin (Fig. 1a). Further south, the plate-boundary zone passes through continental crust, forming a wide transform fault zone, referred to as the Marlborough fault system, and trends 055°–075° (Fig. 1b & c). Here, the component of instantaneous relative plate motion parallel to the plate-boundary zone is greater than the normal component. The instantaneous rotation pole and rate of Chase (1978) are used in this study.

The kinematics and structural evolution of the Marlborough fault system are of general significance for the understanding of rotational deformation in continental crust. This paper describes in detail the last 25 Ma of deformation in part of the Marlborough fault system, and then discusses more regional aspects of the deformation. Emphasis is placed on the pattern of horizontal deformation in the brittle crust.

MARLBOROUGH FAULT SYSTEM

The Marlborough fault system comprises five major faults (Wairau, Awatere, Clarence, Kekerengu and Hope faults, Lensen 1962) (Fig. 1c) which extend for over 100 km and are spaced 5–20 km apart, defining fault blocks such as the Wairau block (region between the Wairau and Awatere faults) and Awatere block. A distributed zone of folding and faulting occurs south of the Hope fault (Fig. 1b). During the last 10 Ka, the slip vectors of the major faults indicate predominantly dextral strike-slip motion with average strike-slip rates between 4 and 15 mm a^{-1} (Berryman 1979, Kieckhefer 1979, Wellman 1983, Grapes & Wellman 1986) and total strike-slip displacements on individual faults between 5 and 50 km (Lensen 1962, this study).

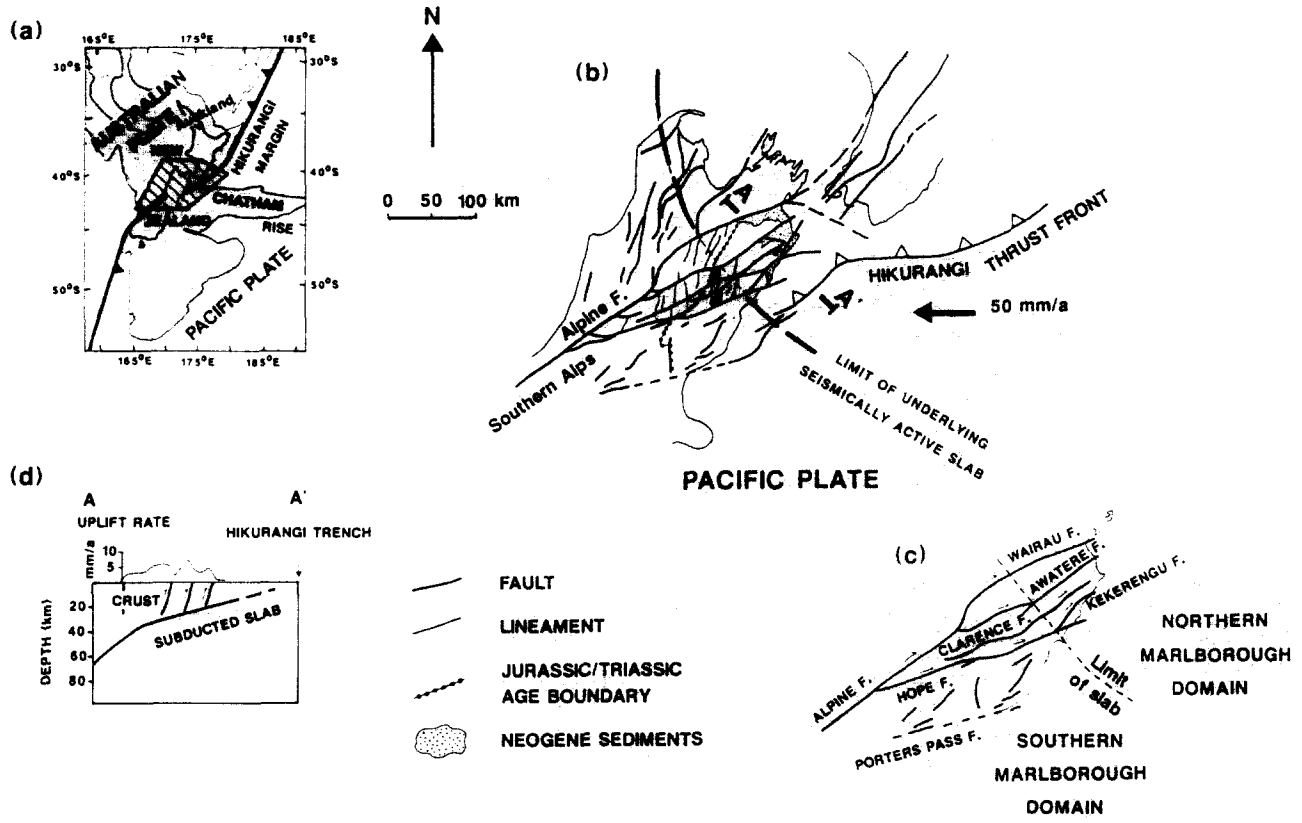

Fig. 1. (a) Regional setting of New Zealand plate-boundary zone between the obliquely convergent Australian and Pacific plates, showing areas of continental crust (stippled). Box with diagonal shading shows region shown in (b). (b) General tectonic map of the New Zealand plate-boundary zone in the northern part of the South Island, New Zealand (modified from Lensen 1962, New Zealand Geological Survey 1972, Lewis 1985). Cross-section AA' shown in (d). Large arrow shows relative plate convergence vector (50 mm a^{-1}). (c) Map of the Marlborough fault system, showing the division into the northern and southern Marlborough domains, based on the change in trend of the major faults. This coincides with the southern limit of the underlying seismically active subducted Pacific plate. (d) Cross-section (Robinson 1986) along line AA' in (b), showing the location of the subducted slab at a depth of 20–30 km, the major faults and the pattern of uplift deduced from a summit height surface with a nominal age of 250 Ka (discussed in text).

Two domains within the Marlborough fault system are distinguished in this study, based on a distinct change in the trend of the major faults (Fig. 1c). In the northern Marlborough domain the faults trend *ca* 055°, compared with *ca* 070° in the southern Marlborough domain. The latter trend within 20° of the instantaneous vector of relative plate motion (Chase 1978). The seismically active subducted Pacific plate underlies the northern Marlborough domain (Figs. 1b–d) and its southern edge approximately coincides with the boundary between the two domains (Walcott 1979, Ansell & Adams 1986).

Study area

About 100 km^2 of complexly deformed Cretaceous and Tertiary sediments have been mapped in detail in the region between the northern end of the active ENE-trending Hope fault and the active NE-trending Kekerengu fault, near the boundary between the northern and southern Marlborough domains (Fig. 2). The stratigraphy is summarized in Fig. 3, with ages based on microfossil dating (Lensen 1962, Prebble 1976, Osborne 1980, this study). An essentially parallel sequence of deep water and marine Upper Cretaceous to Pliocene sediments including limestone, referred to as cover rocks, rest with marked angular unconformity on older deformed and indurated Mesozoic flysch deposits, referred to as basement (Fig. 3). A thick sequence of Miocene conglomerates and turbidites, referred to as the Great Marlborough Conglomerate, contains angular and rounded clasts of all older lithologies.

Structure

The pattern of deformation can be used to divide the study area into nine structural domains, labelled A–I (Fig. 5). Several generations of deformation structures have been recognized in the study area, which are labelled in a sequential manner: foliations (S_1–S_2); fold phases (F_1–F_4); fault generations (T_1–T_3). These can be readily grouped into two deformation phases; an early deformation, which occurred in the Miocene, labelled D_1; a later Plio-Pleistocene deformation, which is also active today, labelled D_2.

EARLY DEFORMATION (D_1)

D_1 deformation comprises S_1, F_1, T_1 structures, which are mainly observed in limestones. The S_1 foliation is

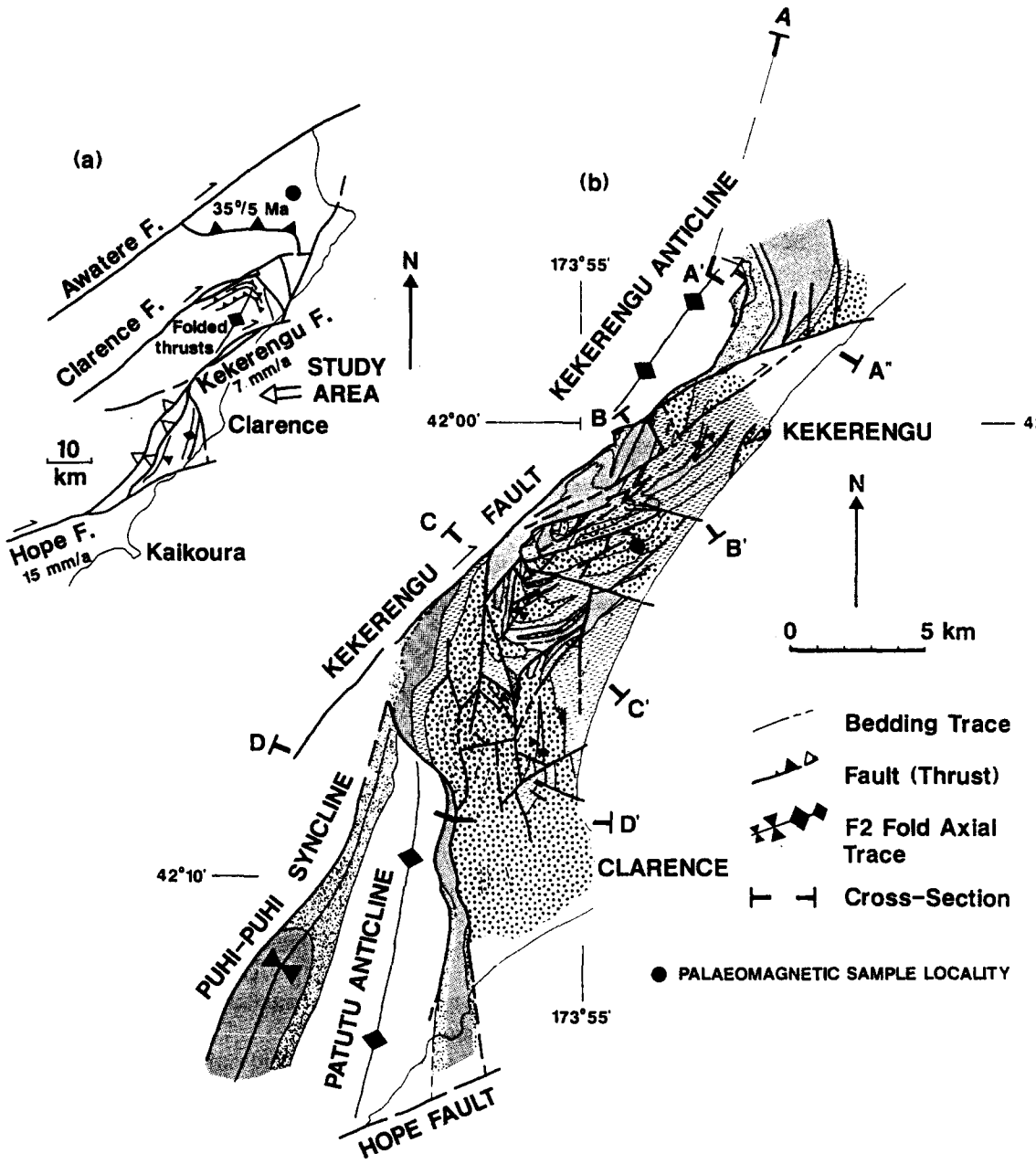

Fig. 2. (a) Map of the major structures between the Awatere and Hope faults. Note both the change in trend of the major faults and folded thrusts. The study area forms the region to the SE of the Kekerengu fault. (b) Geological map of the study area. See Fig. 3 for key to stratigraphic units. Cross-sections are shown in Fig. 4.

found in limestones throughout the study area, including those which form part of parallel sequences resting unconformably on Mesozoic basement, and occurs as stylolitic seams at a low angle (up to 20°) to bedding and associated with calcite veins. In places, this foliation pre-dates the Middle Miocene Great Marlborough Conglomerate, as the orientation of the foliation in limestone clasts is not consistent, and the foliation is truncated at clast margins. Lower Tertiary limestone units are sometimes internally folded into m-scale tight to isoclinal steeply plunging F_1 folds, which contain a weak axial planar foliation.

Structural repetition (T_1)

Upper Cretaceous to Middle Miocene stratigraphic sequences are often repeated along contacts (T_1) which are subparallel to the lithological layering (Figs. 2b and 4). Thrust faults in Domain A are generally at a low angle to bedding and cut up through the stratigraphic section towards the E or SE with a flat and ramp geometry with displacements of several km (cross-section AA'A" in Fig. 4) (Prebble 1976). The thrust planes are clearly folded by a major D_2 anticline (F_2 Kekerengu anticline). In Domain F, a sequence from Lower Tertiary limestone to Middle Miocene Great Marlborough Conglomerate, up to 1 km thick, occurs three times (cross-section CC' in Fig. 4). Repeated sequences can be traced along strike for more than 5 km and are folded by the F_2 Kekerengu syncline.

The localized occurrence of limestone–breccia conglomerates in the Great Marlborough Conglomerate immediately below and adjacent to km-scale alloch-

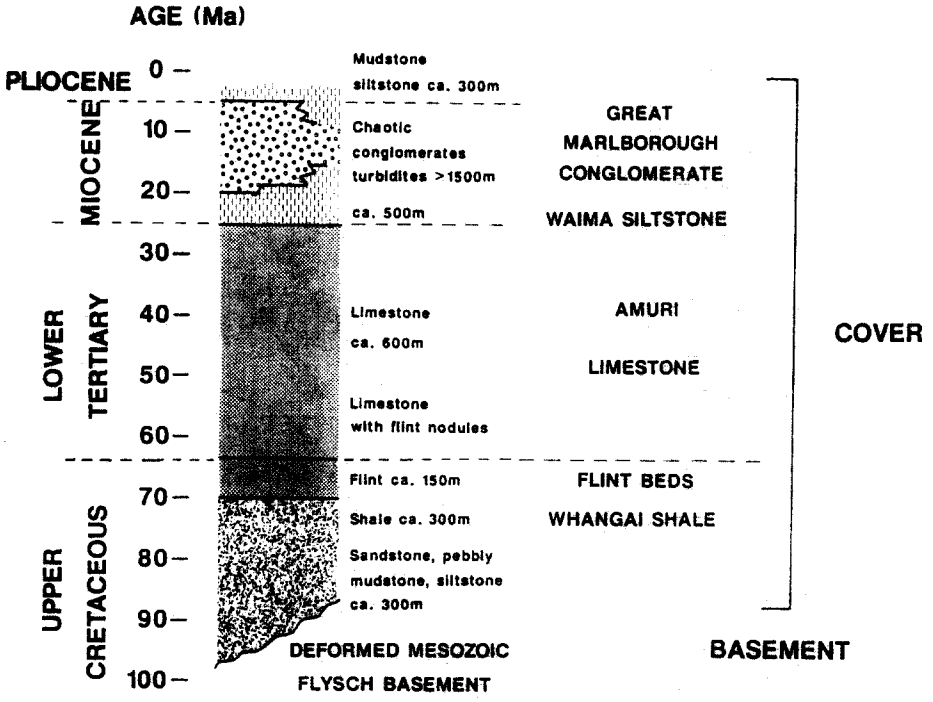

Fig. 3. Informal stratigraphy of the study area. The definition of Amuri Limestone differs from that of other workers (Browne & Field 1985) and includes intercalated Oligocene volcanics (rare in the study area) and limestone above a possible Oligocene disconformity (Browne & Field 1985). In the study area, a conformable transition is observed between Lower Tertiary limestones and Lower Miocene siltstones and mudstones, referred to as the Waima Siltstones. The latter are conformable and interfinger with Miocene Great Marlborough Conglomerate, which passes up into Pliocene mudstones and siltstones. However, the presence of Upper Miocene strata has not been proved in the study area.

thonous limestone units, and also the lack of shearing in the underlying Great Marlborough Conglomerate (localities 1–3 in Figs. 6 and 7a), suggest that the allochthonous sequences form synsedimentary high-level thrust sheets. These may have slid locally along the sediment–water interface, with the development of screes which were subsequently overridden.

Regional deformation

The Great Marlborough Conglomerate and Waima Siltstones (Fig. 3) were deposited in a near-shelf submarine fan complex (Lewis & Laird 1981) and form a markedly different sedimentary facies to that of the limestone in the underlying Lower Tertiary sequences. This change may mark the onset of D_1 deformation at 20–25 Ma. The submarine fan sequences are situated near the boundary between the two Marlborough domains. The Great Marlborough Conglomerate is poorly developed to the northeast of the study area, and also south of the Hope fault. However, a fault-bound sliver is found in the Awatere fault zone (Lensen 1962), suggesting that Great Marlborough Conglomerate was deposited in the Awatere block. Thus, the presence of D_1 structures in clasts within the Great Marlborough Conglomerate, as well as the deposition of the conglomerate itself, suggests considerable deformation and uplift elsewhere during and prior to the Middle Miocene, probably in the regions which are presently further west (Wairau block), while sedimentation continued in the Awatere block and the study area (Fig. 9). Evidence for D_1 deformation is also found immediately south of the study area, where an S_1 foliation is found in Upper Oligocene limestones at Kaikoura, near the northern end of the Hope fault. However, D_1 deformation fabrics have not been reported from the southern Marlborough domain.

At the northern ends of the Wairau and Awatere blocks, a gently dipping and conformable sequence of Upper Miocene to Pliocene sediments (Kennett 1966) rests with angular unconformity on Mesozoic basement (Figs. 1b and 9). Thus, deformation, uplift and erosion in the Awatere and Wairau blocks may have occurred between the Middle and late Miocene (*ca* 15–10 Ma). In addition, low-angle thrust faults in the study area, such as the ramp and flat thrusts in Domain A (Prebble 1976), developed prior to the Plio-Pleistocene D_2 deformation.

LATE DEFORMATION (D_2)

D_2 comprises deformation which distorts D_1 structures, and is active today. Locally, several generations of D_2 structures are recognized (S_2, F_2–F_4, T_2–T_3), which deform Pliocene strata to the same extent as Miocene strata and therefore formed in the last 4 Ma. A measure of the nature and intensity of D_2 deformation in the study area is given by a histogram of bedding dips (Fig. 10), regardless of strike, which has a mode of *ca* 85°, mean of *ca* 70° and a standard deviation of 34°. About 20% of measured strata are overturned.

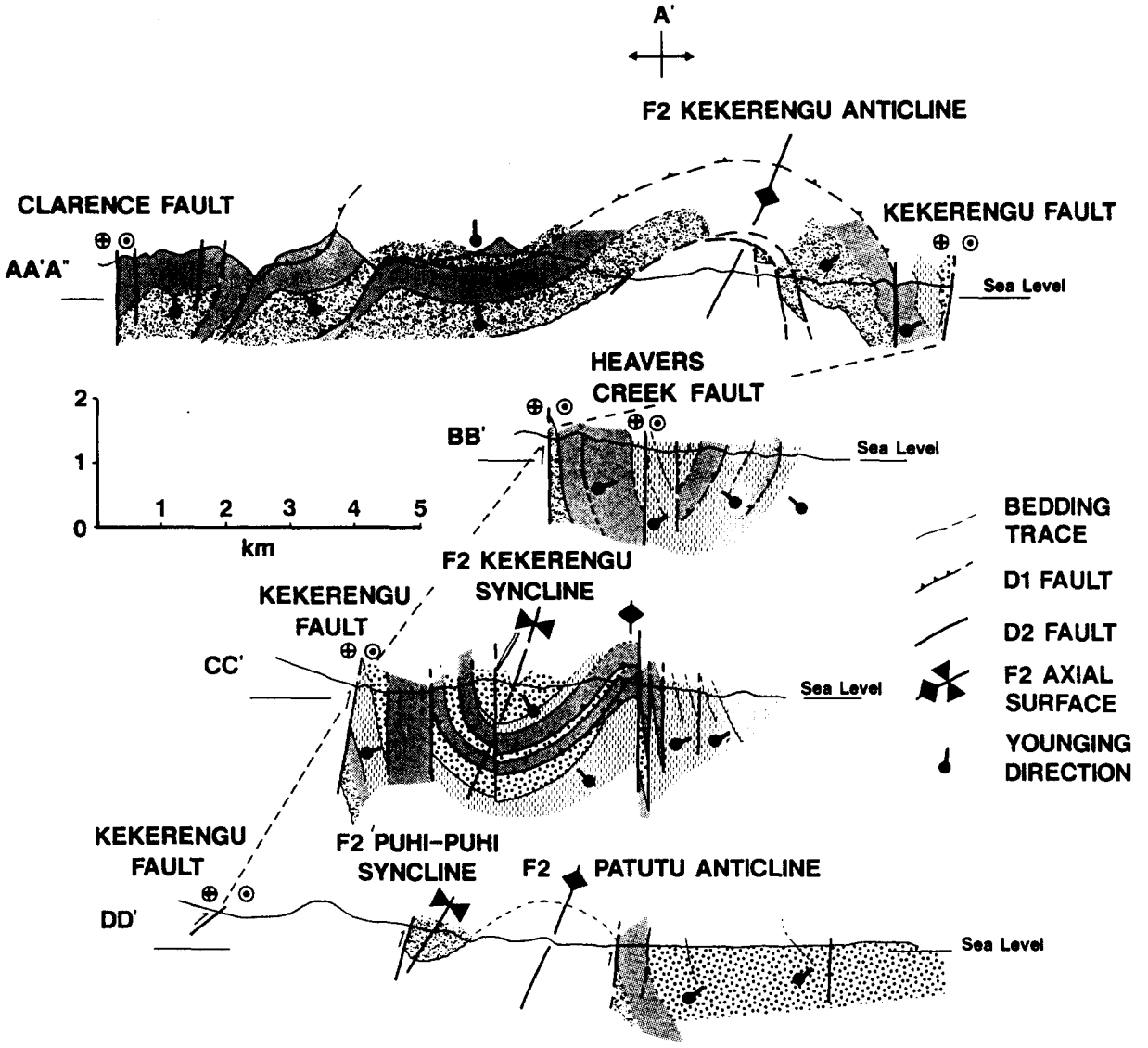

Fig. 4. Cross-sections through the study area. See Fig. 2(b) for location, and Fig. 3 for key to stratigraphic units. Part of cross-section AA'A", between A and A', is modified from Prebble (1976).

Early folding (F_2)

F_2 folds have wavelengths on km- to cm-scales and deform both S_1 and T_1 structures and Pliocene strata. Cross-section CC' in Fig. 4 suggests that F_2 has accommodated at least 2 km of shortening across the study area. Kilometre-scale F_2 folds have axial traces which are markedly oblique to the Kekerengu and Clarence faults. Metre- to cm-scale folds, with the appropriate asymmetry, occur within limestone in the hinge regions of major F_2 folds. These fold the S_1 stylolitic foliation and also calcite veins, but are associated with an axial planar S_2 pressure solution cleavage, which transects S_1 seams and can be locally traced from limestone clasts into the mudstone matrix of the Great Marlborough Conglomerate.

Domains A, B and I form N–NE-trending and plunging (up to 30°) anticlines, referred to as the Kekerengu and Patutu anticlines, defined by the orientation of the cover sequences with a core of Mesozoic basement (Figs. 2, 4 and 5). Domains D, E and F form a faulted steeply plunging and tight km-scale NNE–NE-trending syncline (Kekerengu syncline, Figs. 2 and 5; cross-sections BB' and CC' in Fig. 4). The plunge of the fold progressively decreases from *ca* 60° in Domain F to *ca* 20° in Domain D (Fig. 5). The axial plane in Domains F and E dips *ca* 60° NW. Subsidiary tight to open NNE-plunging (20–30°) synclines and anticlines within Domain D have wavelengths of the order of 200 m.

Later folding (F_3 *and* F_4)

F_3 folds distort F_2 fold axes. On a regional-scale this appears as a marked swing in trend of the F_2 axial trace from a northerly trend in Domain I and part of G to a NNE–NW-trend in Domains F, E, D and A (Figs. 5 and 12). Stereographic plots of poles to bedding from Domains D and G are spread out along small circles near the perimeter of the stereogram (Fig. 5), suggesting that F_3 folds are a result of rotation about subvertical axes.

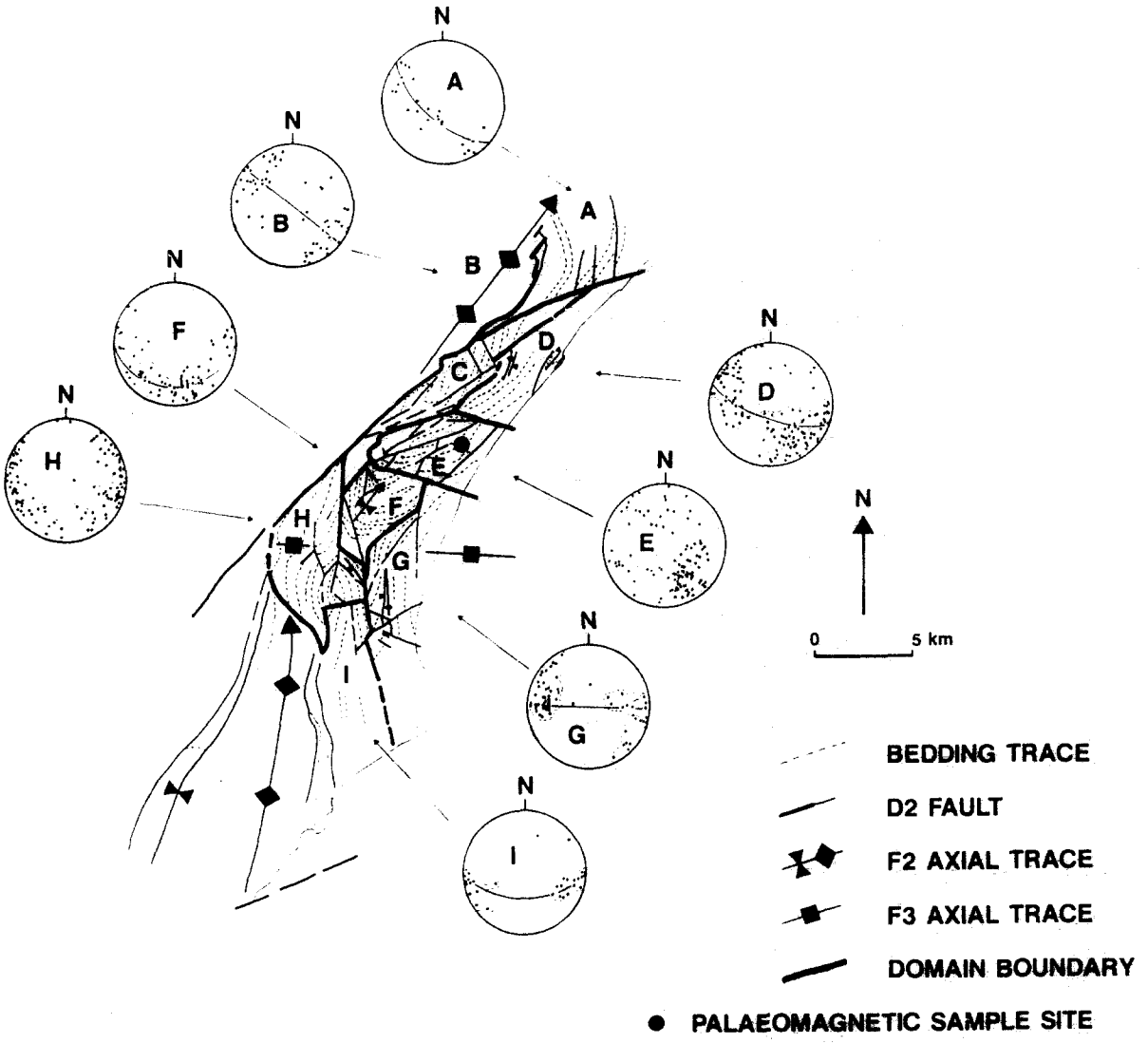

Fig. 5. Structural map of the study area, showing location of domains and equal-area lower-hemisphere stereograms of poles to bedding for the various domains. Some stereograms also show best-fit great circles to poles to bedding, which give the orientation of the major D_2 fold structures. Note the large scatter of points, which are spread out along small circles. This is interpreted as a consequence of folding about subvertical axes (F_3). Palaeomagnetic sample site (clockwise rotation about a vertical axis of *ca* 100° for 18 Ma sediments) is also shown.

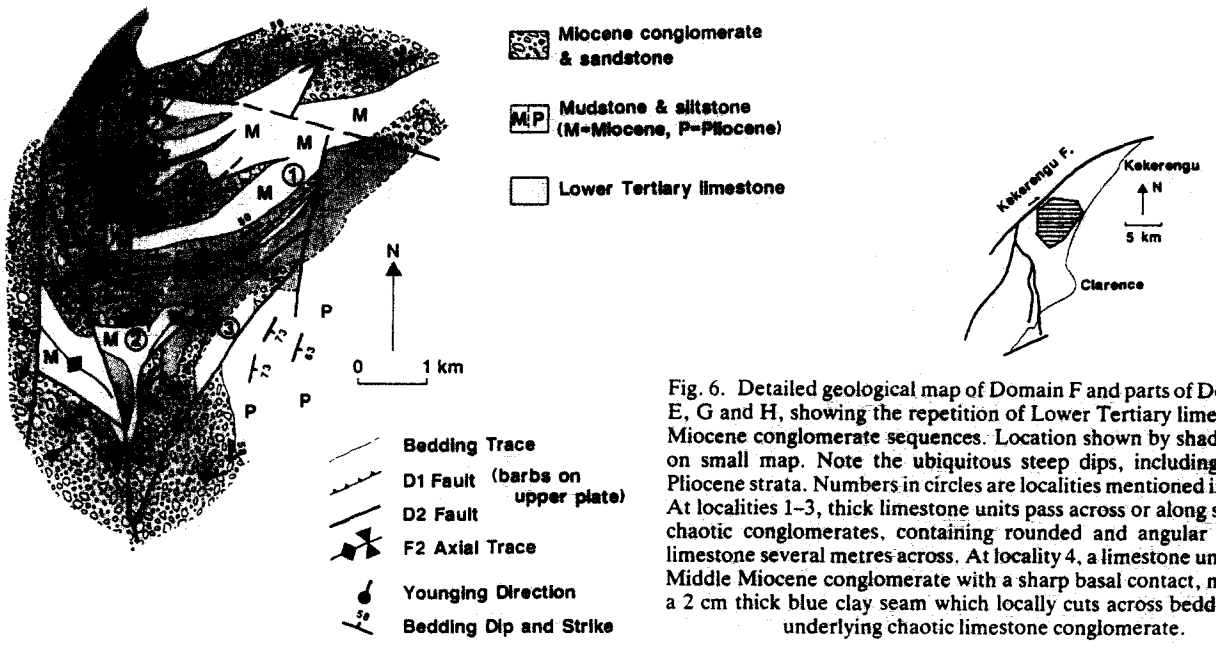

Fig. 6. Detailed geological map of Domain F and parts of Domains C, E, G and H, showing the repetition of Lower Tertiary limestone and Miocene conglomerate sequences. Location shown by shaded region on small map. Note the ubiquitous steep dips, including those in Pliocene strata. Numbers in circles are localities mentioned in the text. At localities 1–3, thick limestone units pass across or along strike into chaotic conglomerates, containing rounded and angular blocks of limestone several metres across. At locality 4, a limestone unit rests on Middle Miocene conglomerate with a sharp basal contact, marked by a 2 cm thick blue clay seam which locally cuts across bedding in the underlying chaotic limestone conglomerate.

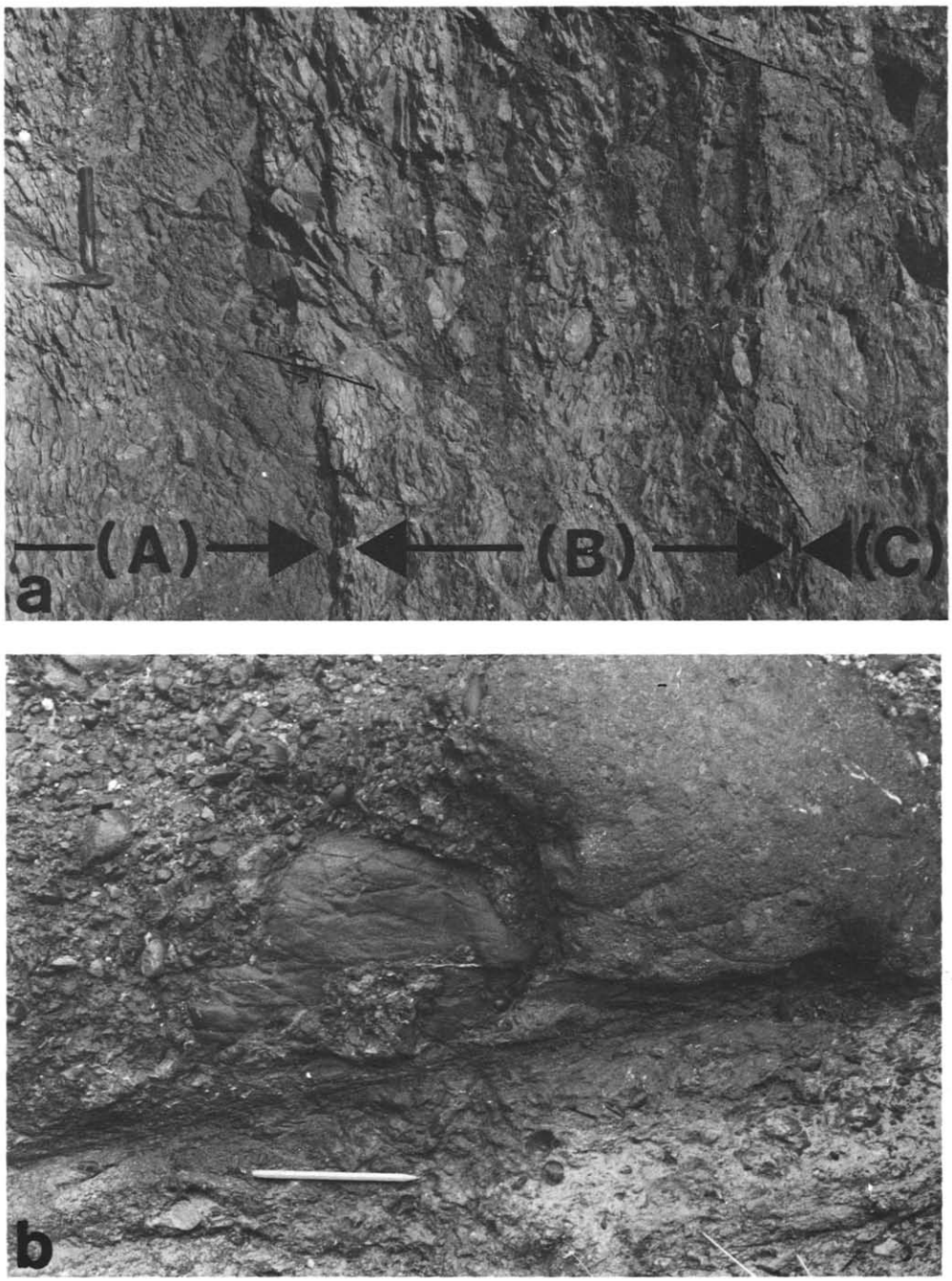

Fig. 7. (a) View of vertical exposure (locality 1 in Fig. 6) of contact zone between allochthonous Lower Tertiary limestone (zone C in picture) and underlying Middle Miocene pebbly mudstone (zone A in picture). A 1–2 m wide zone of intercalated limestone breccia and mudstone layers (zone B in picture), with isolated undeformed sandstone pebbles (up to 10 cm across), occurs immediately below the *ca* 100 m thick limestone unit. Note tens of cm offsets on T_3 faults. (b) View of horizontal exposure of small-scale dextral strike-slip T_2 faults which offset clasts in the Great Marlborough Conglomerate (locality 10 in Fig. 12).

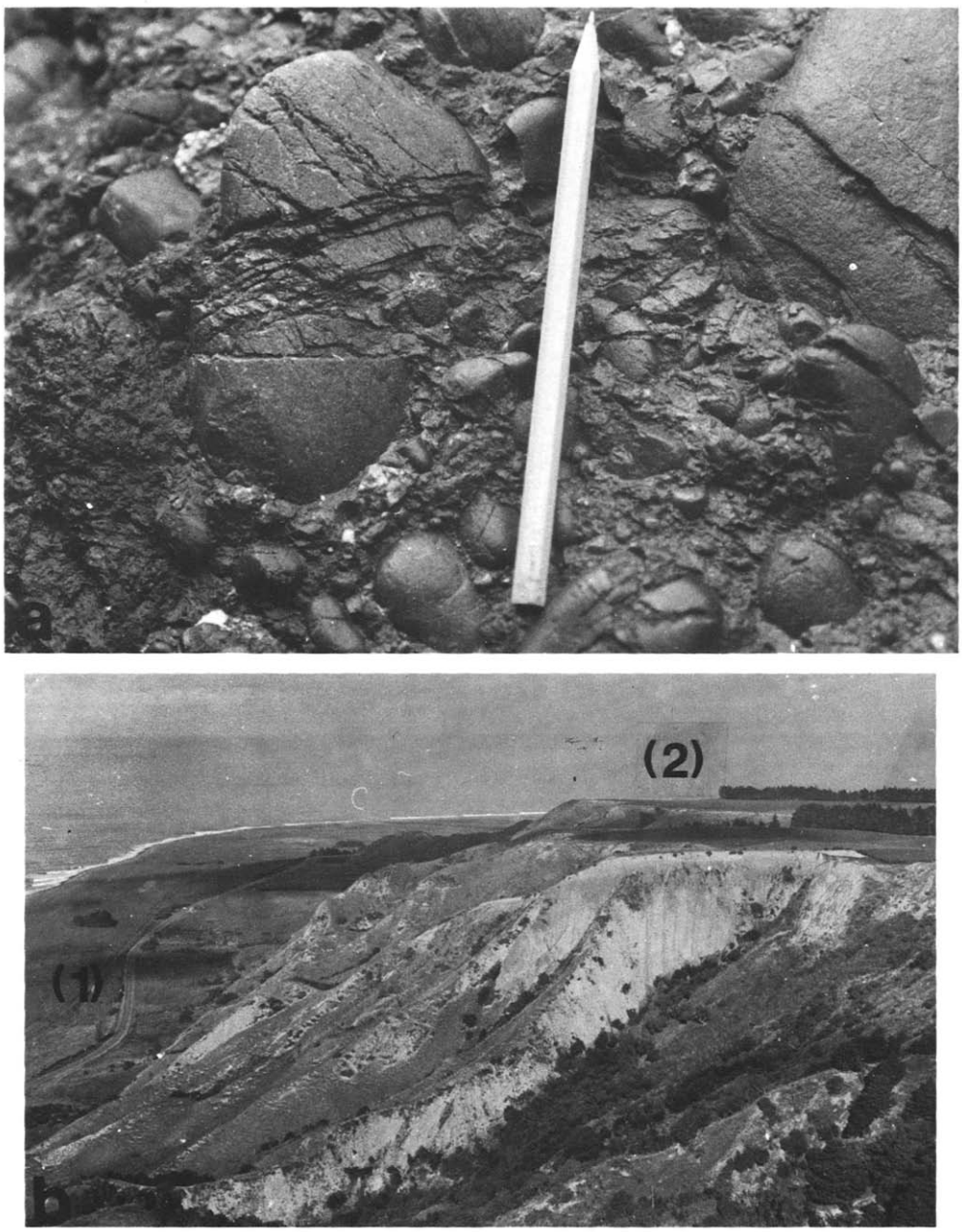

Fig. 8. (a) Indurated and fractured sandstone pebble in Great Marlborough Conglomerate. Note the two sets of fractures (locality 10 in Fig. 12). (b) Marine terraces near the mouth of the Clarence river (locality 6 in Fig. 12). The lower region (labelled 1), at the foot of the cliffs, is the result of Holocene marine erosion and deposition, consisting of a series of raised beaches and alluvial fans. The higher surface (labelled 2), at the top of the cliffs, is underlain by up to 30 m of mainly marine and poorly consolidated sediments, referred to as the Parikawa formation and assumed to have been deposited between 60 and 125 Ka b.p.

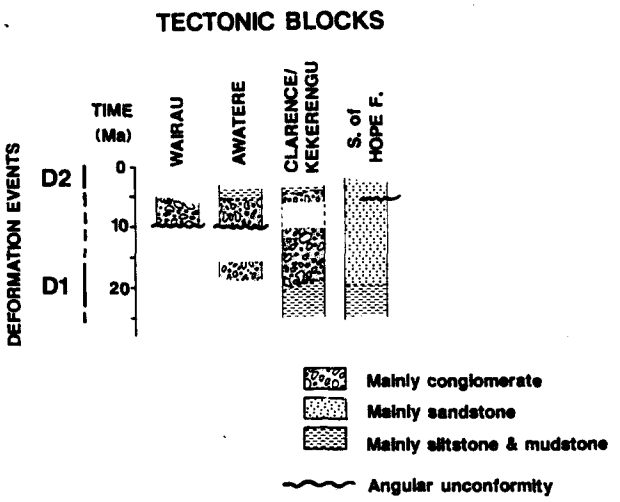

Fig. 9. Diagram illustrating the deformational and sedimentary history of various tectonic blocks in the northern Marlborough domain and south of the Hope fault.

Open m- to tens of m-scale F_4 folds have subhorizontal axial planes and fold steeply dipping units, showing up as a variation in tilt with altitude. These folds may be a result of superficial gravitational collapse.

Large scale faults (T_2)

F_2 structures and Pliocene strata in the study area are offset by km-scale subvertical faults. A rose diagram of the trends of these faults (Fig. 11) suggests a trimodal pattern: set (1) trending *ca* 050°; set (2) trending *ca* 350°; set (3) trending *ca* 290°. The cumulative lengths of sets (1) and (2) faults are similar, though set (2) faults have shorter individual lengths. Set (3) faults (for instance locality 4 in Fig. 12) form the boundaries between Domains D, E, F and G. The fault sets define blocks less than 5 km across, suggesting distributed deformation across the study area. Sets (1) and (2) faults are clearly conjugate as each deforms the other.

Dextral strike-slip offsets have been recorded on a number of set (1) faults. The Kekerengu fault (Figs. 2b and 12) has a remarkably straight trace extending for at

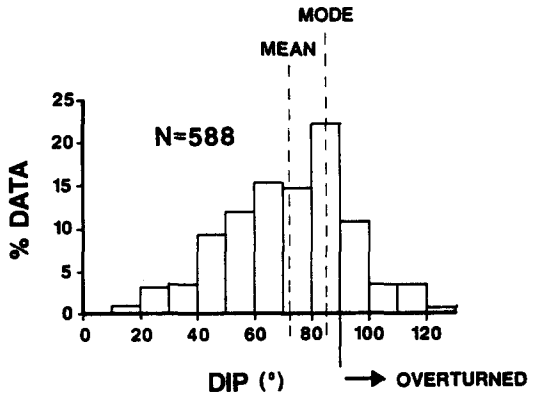

Fig. 10. Histogram of bedding dips including those in Pliocene strata, regardless of strike, in the study area (588 measurements). Note that *ca* 20% of the measured strata are overturned.

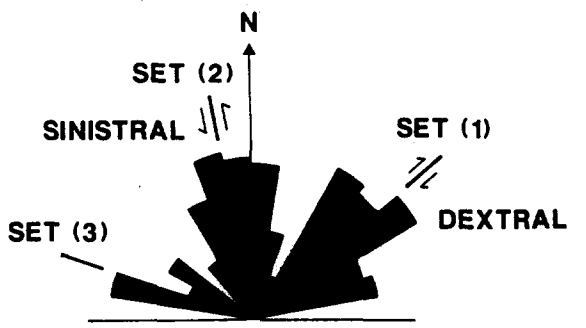

Fig. 11. Rose diagram of trends of km-scale steeply dipping faults, plotted as cumulative length with a 10° azimuth window. Cumulative length is proportional to area of rose diagram.

least 20 km and trending *ca* 050°, separating Mesozoic basement from cover sequences. Further north, where cover rocks outcrop on both sides, its strike swings round to *ca* 065°. It has a clear topographic expression suggesting that it is a reverse fault dipping steeply (>60°) to the NW. The Heavers Creek fault runs essentially parallel to the Kekerengu fault, and also has a good topographic expression suggesting a subvertical fault, upthrown on the SE side. The Kekerengu and Heavers Creek faults both offset a distinctive and subvertical Upper Cretaceous to Miocene sequence, each with a few km of dextral strike-slip displacement (Figs. 2b and 12).

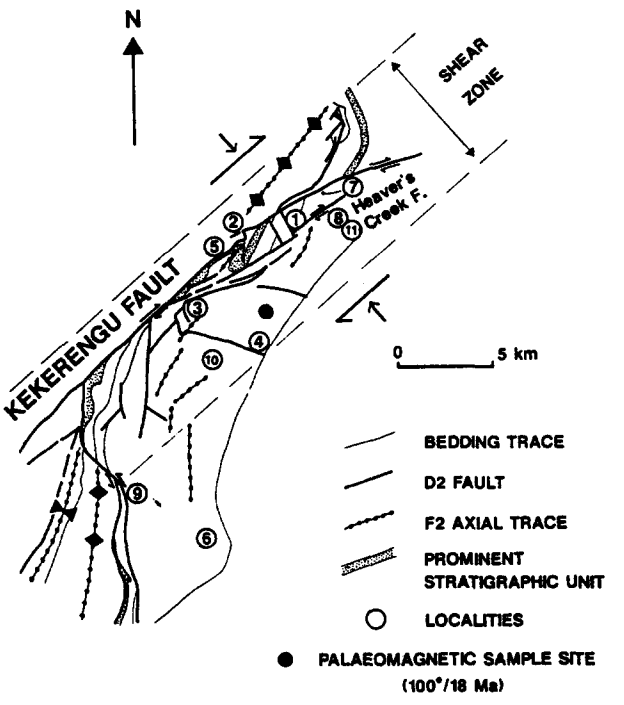

Fig. 12. Structural map of the study area showing major fault and fold trends, and localities (numbers in circles) mentioned in text. Note the sinistral side-steps or jogs of the Kekerengu and Heavers Creek faults (localities 1 and 2). At locality 3, an originally NW-trending sinistral fault appears to have been truncated and locally rotated into parallelism with a NE-trending dextral fault. A prominent and steeply dipping Cretaceous stratigraphic unit is displaced several km across the major faults. This unit is folded into a km-scale steeply plunging Z-shaped fold structure between the Kekerengu and Heavers Creek faults at locality 5. Palaeomagnetic sample site is also shown. Thin dashed lines show the approximate limits of intense dextral shear, defining a shear zone which is modelled (see text).

Sinistral strike-slip offsets have been recorded on a number of set (2) faults (for instance localities 1–3 and 9 in Fig. 12). The offset of a subvertical Lower Tertiary stratigraphic sequence across a N–NW-trending fault (locality 9 in Fig. 12) suggests 1–2 km of sinistral strike-slip movement. This fault is active as it has a pronounced topographic fault scarp with a marked difference in the height of Holocene river terraces either side of the fault.

Small scale faults (T_2)

Metre- to cm-scale subvertical faults are ubiquitous and mirror the pattern of the km-scale T_2 faults (Fig. 7b). In addition, indurated sandstone pebbles in the Great Marlborough Conglomerate, within a few hundred metres of the major faults, are commonly fractured (Fig. 8a). This fracturing may have occurred simultaneously with the earthquake rupture of the adjacent km-scale fault, perhaps accommodating internal deformation in the hangingwall or associated with folding. The total finite deformation as a consequence of micro-fracturing may be significant, resulting in a shear strain up to 10^{-1}.

Late faults (T_3)

Conjugate reverse faults commonly offset subvertically dipping strata up to several metres, resulting in subvertical extension and subhorizontal shortening (Fig. 7a). These faults may represent a late stage of shortening when folds were sufficiently tightened that further folding could not accommodate much shortening.

Distributed deformation

Bedding planes near major T_2 faults show a marked rotation into parallelism with the generally subvertical fault plane. In addition, Upper Cretaceous–Lower Tertiary shales, flint beds and limestone, between the dextral strike-slip Kekerengu and Heavers Creek faults, form a km-scale steeply plunging Z-shaped fold structure which has an asymmetry consistent with an horizontal dextral shear couple across Domain C (locality 5 in Fig. 12). The flint beds are thickened in the hinge zones and, along with the shale, are extremely thinned on the limb adjacent to the Kekerengu fault, so that the same unit may vary in thickness from *ca* 10 to 500 m. Thus, the mode dip of *ca* 85° (mean *ca* 70°) for bedding data from the whole study area (Fig. 10), and also F_3 folding, may be a consequence of distributed deformation closely associated with faulting.

Domains I and G do not contain a fold structure comparable to the NE-plunging F_2 syncline and anticline in Domains F and G (Figs. 2 and 5). The strike and dip of beds often changes abruptly, defining a number of fault bound blocks less than 5 km across (Fig. 13), which may have accommodated the F_2 folding observed further north.

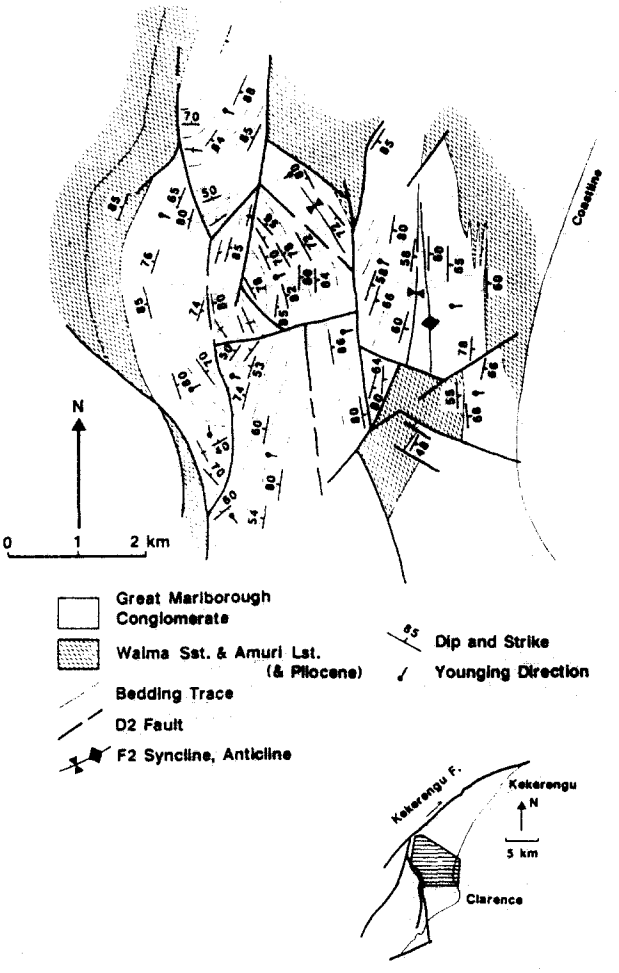

Fig. 13. Map of fault bound blocks in Domains F, G, H and I, defined by abrupt changes in the dip and strike of the Great Marlborough Conglomerate. Note that most strata dip subvertically. Location shown by shaded region on small map.

TECTONIC ROTATION

Early to Middle Miocene (*ca* 18 Ma) sandstones and siltstones in Domain E dip at *ca* 55° NW and form part of a N–NE-plunging (30–60°) synclinal fold structure (Fig. 5). Palaeomagnetic sampling here, after thermal cleaning, has revealed a stable and reversely polarized magnetic field which is considered to represent the Earth's field at the time of formation of these rocks (Figs. 2b, 5 and 12, Mumme & Walcott 1985). Mumme & Walcott (1985) showed that the mean declination of the direction of magnetization, after rotation about the strike of the bedding, bringing the beds to the horizontal, suggested a clockwise rotation of 99 ± 12° about a vertical axis relative to True North. Unfortunately, because of the plunge of the fold structure and the tilt of the fold axial plane, it is not possible to determine an unambiguous rotation of these rocks about a vertical axis. However, corrections taking into account the fold plunge increase the apparent clockwise rotation about a vertical axis obtained by Mumme & Walcott (1985) and suggest that the mean clockwise rotation could be as large as 110°. The rotation of the Pacific plate in the New Zealand

region, relative to True North, has been negligible in the last 80 Ma (Wright & Walcott 1986). Therefore, the palaeomagnetically sampled rocks in Domain E have rotated at least 87° (at the 95% confidence level) clockwise about a vertical axis relative to the Pacific plate in the last 18 Ma.

Some of this rotation may record the 30–40° clockwise swing in trend of F_2 fold axes in the last 4 Ma, described as F_3 folding, consistent with distributed dextral shear across the study area.

SHORT-TERM DEFORMATION

Uplift

In a coastal region which is undergoing uniform tectonic uplift, only marine benches cut during the highest still stands of sea level are likely to be preserved (Mesolella *et al.* 1969). Thus, as has been found in Barbados (Mesolella *et al.* 1969), New Guinea (Chappell 1974) and New Zealand (Ghani 1978) coastal benches, covered by marine deposits, were cut during particular periods, such as between 0 and 6.5 Ka, 30 and 50 Ka, 60 and 125 Ka, corresponding to eustatic sea level maxima.

Three prominent and successive coastal terrace levels occur in the study area. The lowest is at the foot of the coastal cliffs, where the highest beach ridge is assumed to have formed 6.5 Ka b.p. (Fig. 8b, Wellman 1979). Above the Holocene terraces, at the mouth of the Kekerengu River (locality 11 in Fig. 12), tens of metres of gravels with abundant limestone fragments, referred to as the Winterholme Formation (Suggate *et al.* 1978), rest on a subhorizontal bedrock surface *ca* 35 m above sea level, which is assumed to have been cut between 30 and 50 Ka (Chappell 1974). At higher levels, a distinct sequence of mainly marine and poorly consolidated gravels, sands and silts, referred to by Suggate *et al.* (1978) as the Parikawa Formation (Fig. 8b, locality 6 in Fig. 12), can be traced along the top of the coastal cliffs to the northeast of the Clarence River. These are assumed to be resting on a marine bench cut between 60 and 125 Ka (Ghani 1978). The heights of these surfaces above sea level (Table 1), taking into account eustatic sea level changes (Chappell 1974), suggest uplift rates between 0.8 and 2.5 mm a^{-1}. McFadgen (1987) has deduced a Holocene uplift rate of 1.5 mm a^{-1}, based on ^{14}C dates, for the Kaikoura Peninsula south of the study area. Wellman (personal communication) has deduced a Holocene uplift rate of 1.8 mm a^{-1} at the mouth of the Clarence River, based on ages inferred from the degree of weathering of pebbles.

Wellman (1948, 1979) and Ghani (1974, 1978) noted a marked summit height accordance in the southern part of the North Island and also the Marlborough region. Changes in the summit heights coincide with major active fold and fault structures in both the southern part of the North Island and the Marlborough region (Wellman 1948, 1979, Ghani 1974, 1978, Kieckhefer 1979, Lamb & Vella 1987, this study). In the southern part of the North Island, Ghani (1978) showed that there was a good correlation between the altitude of the summit heights and the uplift rates for the last *ca* 100 Ka. Thus, the summit heights were considered to represent the remains of a wave-cut surface, with a nominal age of 250 Ka (Wellman 1979). This age provides a powerful means of deducing uplift rates away from the coast (Fig. 14). It is possible that the summits heights did not in fact form an originally planar surface of the same age, but are the remains of a region of low relief that was close to sea level between 200 and 300 Ka. If the original relief did not exceed 250 m, then the maximum uplift rates contoured in Fig. 14 will not be in error by more than 3 mm a^{-1}, and lower uplift rates will be in error by less than this.

Figure 14 suggests that most of the study area, averaged over 250 Ka, forms a region uplifting between 1 and 2 mm a^{-1}, consistent with the uplift rates deduced for the last 100 Ka, surrounded by rapidly uplifting Mesozoic basement.

Tilting

The variation in uplift rate indicates a regional plunge (6° Ma^{-1}) towards the NE and roughly parallel to the trend of F_2 axial traces. This is consistent with the NE plunge of F_2 folds, and suggests that the plunge of the Kekerengu anticline (*ca* 25°) could have been achieved in 4 Ma. Tilting associated with the rotation of F_2 limbs

Table 1. Uplift data for study area

Feature	Location	Latitude/longitude	Height* (m)	Sea level† (m)	Age‡ (Ka)	Uplift rate (mm a^{-1})
Highest Holocene beach ridge	Mouth of the Clarence River	42°09'S/173°56'E	~15	—	6.5	~2.3
Highest Holocene beach ridge	Mouth of the Kekerengu River	42°00'S/174°00'E	~5	—	6.5	~0.8
Base of Winterholme Formation	Mouth of the Kekerengu River	42°00'S/174°00'E	35	−25 to −40	30–50	1.2–2.5
Base of Parikawa Formation	Mouth of the Clarence River	42°09'S/173°55'E	130	0 to −20	60–125	1.0–2.5

* Height above present day mean sea level.
† Sea level at the time of formation of marine terrace, relative to present day mean sea level, taken from Chappell (1974).
‡ Ages are based on a marine terrace sequence and a correlation with eustatic sea level maxima (see text).

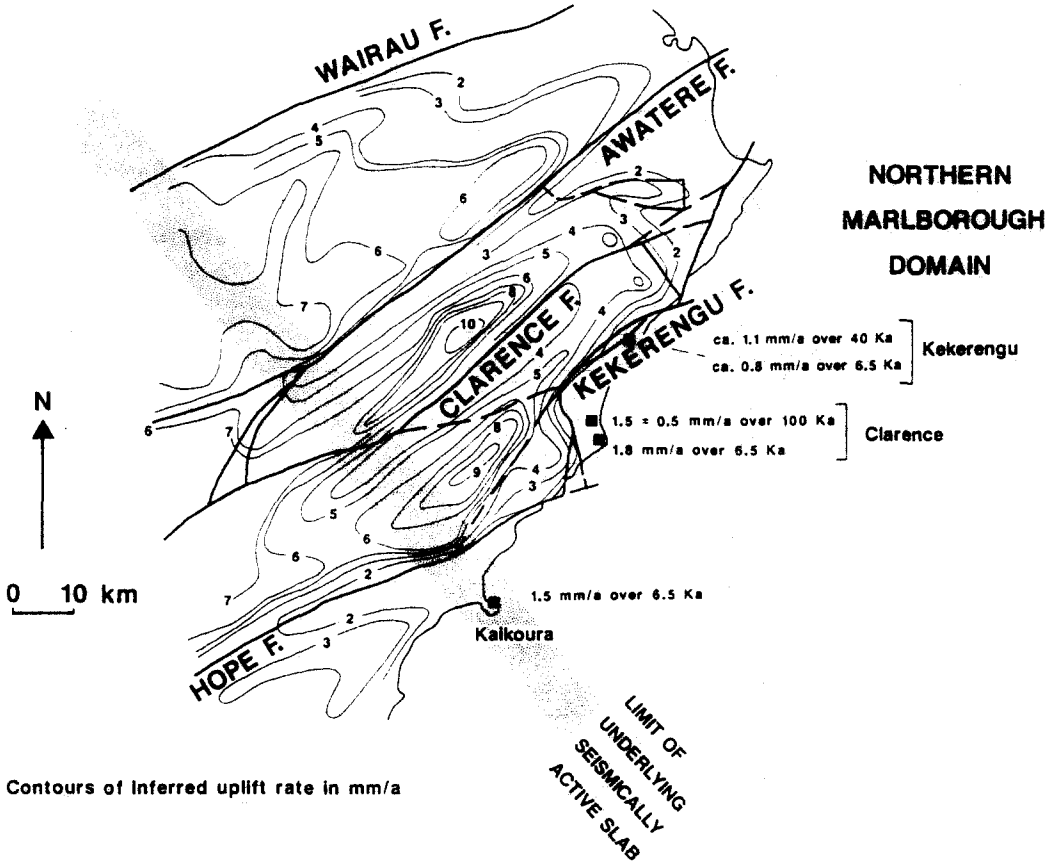

Fig. 14. Map of the northern Marlborough domain and part of the southern Marlborough domain, showing the major faults and contours of estimated uplift rate in mm a^{-1}. Uplift rates are deduced from the altitude of a distinct summit height surface, which is assumed to have been close to sea level 250 Ka ago. Other estimates (solid squares) of uplift rates are also shown (Table 1), and are consistent with those deduced from the summit heights. Note the change in uplift pattern and fault trend across the boundary of the seismically active subducted slab.

Table 2. Fault slip data for the study area

Feature	Location	Latitude/longitude	Fault plane Strike (°)	Fault plane Dip (°)	Displacement Strike-slip* (m)	Displacement Vertical† (m)	Age (Ka)	Reference
Kekerengu Fault								
Winterholme Formation	SW bank of Kekerengu River, 3.5 km from river mouth	41°98'S/173°99'E	065	60–90 NW	300 D		30–50‡	Prebble 1976
River terraces next to the Kekerengu River	SW bank of Kekerengu River, 3.5 km from river mouth		065	60–90 NW		1 (NW)	~7§	This study
	SW bank of Kekerengu River, 3.5 km from river mouth		065	60–90 NW	27 D		~4§	This study
	SW bank of Kekerengu River, 3.5 km from river mouth		065	60–90 NW	4 D	0.3 (NW)	⩽10	Wellman 1983
Heavers Creek Fault								
Parikawa Formation	NE side of Heavers Creek, 2 km from river mouth	42°00'S/173°59'E	055	90	25 D	6 (SE)	100‡	This study

* D = dextral strike-slip displacement.
† Upthrown side down shown in brackets.
‡ Estimated age based on sequence of uplifted marine terraces (see text).
§ Calculated assuming downcutting rate of the Kekerengu River on the SE side of Kekerengu Fault is the same as the uplift rate on the same side of the fault, estimated at 1 mm a^{-1}.

cannot be resolved. However, the mean stratal dip is *ca* 70°, which suggests an average tilt rate for the last 4 Ma of *ca* 18° Ma^{-1}, comparable to that for the Hikurangi margin in the southern part of the North Island (*ca* 15–20° Ma^{-1}, Lamb & Vella 1987).

Fault slip rates in the study area

The margins of the region of relatively low topography in the study area (<500 m a.s.l.) coincide with major faults. The offsets of terraces, cut by the faults, can be used to deduce slip rates on the faults, if the ages of the terraces are known (Table 2). The Kekerengu fault offsets a series of river terraces adjacent to the Kekerengu River, each by different amounts (locality 7 in Fig. 12, Table 2). If one makes the simplest assumption that the downcutting rate of the river equals the uplift rate, deduced from uplifted marine terraces to be *ca* 1 mm a^{-1} for the downthrown side of the Kekerengu fault at this locality, then these offsets (Table 2) suggest an average Holocene dextral strike-slip rate of *ca* 7 mm a^{-1}, and a vertical slip rate of 0.15 mm a^{-1} (Table 2). A *ca* 300 m dextral strike-slip offset of the Winterholme Formation (Table 2) (Prebble 1976), taken to be 30–50 Ka old using uplifted marine terrace chronology, suggests an average dextral strike-slip rate over this period between 5 and 10 mm a^{-1}.

The Heavers Creek fault offsets a surface (locality 8 in Fig. 12, Table 2) underlain by the Parikawa Formation (Lensen 1962, Suggate *et al.* 1978), assumed to have been deposited between 60 and 120 Ka. It follows that the average vertical displacement rate on the Heavers Creek fault is *ca* 0.06 mm a^{-1} and the average dextral strike-slip rate is *ca* 0.25 mm a^{-1}(Table 2). The estimated slip rate on the Kekerengu fault is significantly faster than that on the Heavers Creek fault, and their estimated combined strike-slip rate is *ca* 7.5 mm a^{-1}.

Geodetic deformation

Triangulation surveys were carried out in the study area in both 1882 and 1896. Stations established in these surveys were reoccupied in 1983. A comparison of the different surveys, using the method of simultaneous reduction (Bibby 1981) and assuming no slip on the faults, has shown that tectonic deformation has occurred since the early surveys. The derived shear strain rates for various networks within the study area are shown in Table 3 and Fig. 15. The azimuth of the principal axis of horizontal compression in the study area (networks 2–4) is remarkably constant at *ca* 110°. The azimuth is more southeasterly in networks 1 and 5 (Table 3, Fig. 15). Maximum shear strain rates are between 0.2×10^{-6} and 0.6×10^{-6} a^{-1}.

SHEAR ZONE MODEL

Part of the study area during D_2 deformation can be modelled as a straight and parallel-sided zone of dis-

Table 3. Geodetic strain rate data for networks in the study area (see Fig. 15 for location of networks)

Network	T*	$\dot{\gamma}_1$†	$\dot{\gamma}_2$‡	$\dot{\Gamma}$§	ψ‖
1	101	−0.10 ± 0.10	0.37 ± 0.11	0.38 ± 0.11	127 ± 8
2	87	−0.43 ± 0.08	0.33 ± 0.10	0.54 ± 0.09	109 ± 5
3	87	−0.47 ± 0.08	0.36 ± 0.08	0.59 ± 0.08	109 ± 4
4	87	−0.18 ± 0.07	0.14 ± 0.06	0.23 ± 0.07	109 ± 8
2–4	101	−0.32 ± 0.05	0.30 ± 0.05	0.44 ± 0.05	112 ± 3
5	93	0.02 ± 0.11	0.32 ± 0.11	0.32 ± 0.11	137 ± 10

* Time in years between triangulation surveys.

† $\frac{\partial u}{\partial x} - \frac{\partial v}{\partial y}$ component of shear strain rate (10^{-6} rads a^{-1}) with standard error.

‡ $\frac{\partial u}{\partial y} + \frac{\partial v}{\partial x}$ component of shear strain rate (10^{-6} rads a^{-1}) with standard error,

x = positive to the east (090°)
y = positive to the north (000°)
u = component of velocity along x axis
v = component of velocity along y axis.

For a rotation of axes by θ (anticlockwise positive)

$$\dot{\gamma}_1' = \dot{\Gamma} \cos(2\psi + 2\theta)$$

$$\dot{\gamma}_2' = -\dot{\Gamma} \sin(2\psi + 2\theta).$$

§ Maximum shear strain rate (10^{-6}rads a^{-1}) with standard error,

$$\dot{\Gamma} = (\dot{\gamma}_1^2 + \dot{\gamma}_2^2)^{1/2}.$$

‖ Azimuth from True North of principal axis of compression with standard error, in degrees,

$$\psi = 0.5 \tan^{-1}\left(\frac{\dot{\gamma}_2}{\dot{\gamma}_1}\right).$$

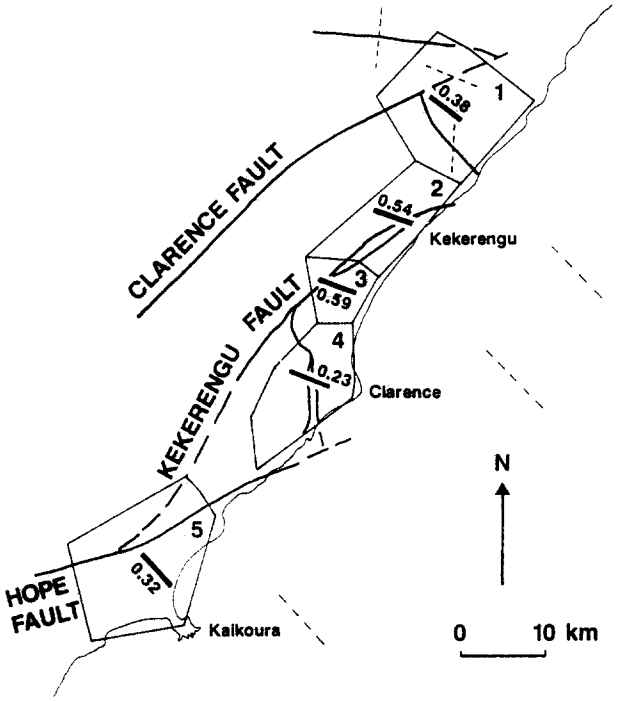

Fig. 15. Map of study area and adjacent regions showing location of the triangulation networks (networks 1–5), which were analysed for horizontal crustal strain over the last *ca* 100 years. The trend of the principal axis of compression (thick bars) and the maximum shear strain rates (in units of 10^{-6} a^{-1}) are also shown (Table 3). Dashed lines are inferred local directions of principal axes of compression, based on an interpretation of the local style of deformation, suggesting predominantly NW–SE compression in the SE near the Hikurangi thrust front, similar to the direction of the relative compressive axis in network 5. Local kinematics may be complicated, and hence strain in triangulation networks (for example in network 1) represents an average.

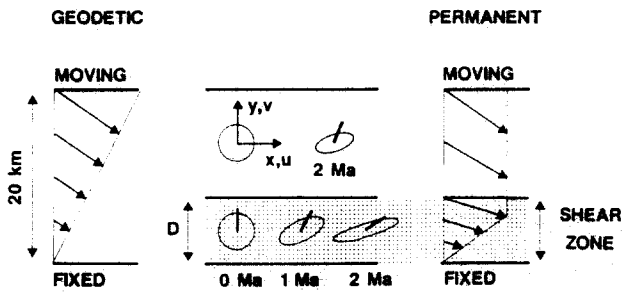

Fig. 16. Definition of parameters used in shear zone model. Geodetic velocity gradients, spread across 20 km, can account for the simple shear component of deformation in the shear zone with width D (ornamented region). Thus, the average $\partial u/\partial y$ velocity gradient of permanent deformation in the shear zone may be 2–4 ($20/D$) times the geodetic velocity gradient. It is assumed that the shortening velocity gradient of permanent deformation in the shear zone is the same as the geodetic one. Also shown are the horizontal finite strain ellipses that would result from deformation over 1 or 2 Ma with either constant geodetic velocity gradients (shown outside stippled shear zone) or estimated average constant velocity gradients of permanent deformation in the shear zone, taking D = 7.5 km. Black bar shows the rotation about a vertical axis of a marker line, initially trending north, painted on a equidimensional rigid crustal block floating in the zone of deformation.

tributed deformation trending 050°, subparallel to the Kekerengu fault (Fig. 12). Taking horizontal axes x, y parallel and perpendicular to the deforming zone, respectively (z axis vertical), the components of velocity of the deforming medium are u, v and w parallel to the x, y and z axes, respectively (Fig. 16). It is possible to compare the various components of long- and short-term deformation (Table 4) if the deforming medium is incompressible, velocity gradients are constant and zero along the length of the deforming zone. The latter assumption is necessary because the geodetic data have neither distance measurements nor an external frame of reference. The components of geodetic strain rate (Table 4) suggest rotational deformation with roughly equal components of dextral simple shear and normal compression. The relative velocity across the study area trends *ca* 085°, subparallel to the plate convergence vector.

Long-term velocity gradients

The geodetic dextral simple shear component across 20 km, which may represent elastic strain in the brittle crust, has a displacement rate equivalent to the estimated combined dextral strike-slip rate on the Kekerengu and Heavers Creek faults (*ca* 7.5 mm a^{-1}). The distribution of D_2 deformation suggests that though dextral shear has been concentrated on the two faults over at least the last 50 Ka, it has been distributed across a shear zone, 5–10 km wide, over several hundred Ka (Figs. 12 and 16). About half of the estimated total dextral shear across the shear zone has been taken up on the two faults. Therefore the average long-term $\partial u/\partial y$ velocity gradient, which has resulted in permanent deformation in the shear zone (including slip on the faults) may be 2–4 times the geodetic $\partial u/\partial y$ velocity gradient (Table 4, Fig. 16); while the part that does not include slip on the faults may be up to twice the geodetic $\partial u/\partial y$ velocity gradient. The shortening velocity gradient ($\partial v/\partial y$) of permanent deformation is assumed to be the same as that determined from geodetic studies (Table 4, Fig. 16).

Floating block model

The rotation rate about vertical axes of small ($\ll$5 km across) isolated crustal blocks can be calculated from the results of Lamb (1987), if the estimated velocity gradients of permanent deformation, excluding slip on the Kekerengu and Heavers Creek faults, describe the velocity field of an underlying and continuously deforming viscous medium on which the crustal blocks are floating (McKenzie & Jackson 1983). Small equidimensional crustal blocks in the shear zone would have rotated clockwise at a rate equal to half the vorticity of the velocity field ($W/2 = 0.5\ \partial u/\partial y$), between 10 and 21° Ma^{-1} (Table 4), although markedly elongate blocks could have had instantaneous rotation rates as high as 45° Ma^{-1}. The average rotation rate will be closer to $W/2$. The inferred local rotation of 30–40° during D_2 deformation could have been achieved in much less than 4 Ma.

Table 4. Components of strain rate in shear zone model

	$\dot{\gamma}_1$*	$\dot{\gamma}_2$†	W‡	$W/2$‡	T§	D‖ (km)	Velocity¶ Strike-slip (mm a^{-1})	Velocity¶ Shortening (mm a^{-1})	Azimuth of relative velocity vector**
Geodetic (100 a)									
Average of networks 2–4 in Fig. 15	0.25	0.37	0.37	0.19	0.13	5–10	1.9–3.7	1.3–2.5	085°
Permanent (100s Ka)	0.25	0.75	0.75 (0.37)	0.37 (0.19)	0.13	10	7.5	2.5	068°
	0.25	1.00	1.00 (0.50)	0.50 (0.25)	0.13	7.5	7.5	1.9	064°
	0.25	1.50	1.50 (0.75)	0.75 (0.37)	0.13	5	7.5	1.3	060°

* $\dot{\gamma}_1 = -\frac{\partial v}{\partial y}$ (units of 10^{-6} rads a^{-1}).

† $\dot{\gamma}_2 = \frac{\partial u}{\partial y}$ (units of 10^{-6} rads a^{-1}).

‡ $W = \frac{\partial u}{\partial y}$ (units of 10^{-6} rads a^{-1}). Rates in brackets exclude slip on the Kekerengu and Heavers Creek faults.

§ $T = -\frac{1}{2}\frac{\partial v}{\partial y}$ (units of 10^{-6} rads a^{-1}).

‖ D is the width of the shear zone (in y direction).

¶ Components of relative velocity of the margins of the shear zone.

** Azimuth of relative velocity vector across shear zone.

Reference frame: x positive trending 050°; y positive trending 320°.

u = component of velocity along x axis; v = component of velocity along y axis; both positive in x or y direction.

Crustal thickening

The relationship between uplift rates and deformation depends on the erosion rate and degree of isostatic compensation. If the athenosphere adjusts instantaneously to the lithospheric load and mass is only changed by erosion, then:

$$kU = 2TH + (k - 1)E, \qquad (1)$$

where U is the uplift rate, $T = 0.5\,\partial w/\partial z = -0.5\,\partial v/\partial y$, H is the crustal thickness, E is the erosion rate (volume/unit area/unit time) and k is a constant, varying between 1 and 6, depending on the degree of isostatic compensation.

The relative proportion of rock volume above sea level, compared with the volume beneath the summit height surface, suggests that E/U is in the range 0.25–0.5 over the last 250 Ka. Using the geodetic data for T (Table 4), and taking an average uplift rate for the study area of 1.5 mm a^{-1} and a crustal thickness of 20 km (Fig. 1d) (Robinson 1986), this suggests nearly full isostatic compensation of the crust, with k between 4 and 6. It may be more reasonable to consider an average uplift rate over a width comparable to the thickness of the crust (*ca* 20 km). In this case, the average uplift rate is *ca* 3 mm a^{-1} (Fig. 14) and k is *ca* 2, similar to that for crust resting on the subducted slab in the southern part of the North Island, in an equivalent position to the study area (Lamb & Vella 1987). Thus, the flexural rigidity of the subducted slab may prevent full isostatic compensation.

Finite strain

Estimates can be made of the horizontal finite strain, if it is assumed that the displacements on the major D_2 faults are equivalent to slip on several sets of parallel faults, oriented parallel to the mean trends of the three fault sets defined in the study area (Fig. 11). However, the rigid-body rotational component of deformation cannot be determined easily without palaeomagnetic data. Field observations suggest that sets (1) and (3) faults have dextral strike-slip components of displacement, and set (2) faults have sinistral strike-slip components of displacement. In addition, the thrust motions on set (1) faults are greater than on set (2) faults, and negligible on set (3) faults.

If strike-slip displacement moments (displacement × fault strike-length) on sets (1) and (2) faults are similar, and negligible on set (3) faults, then the principal compressive axis of the average horizontal finite strain ellipse, as a consequence of strike-slip faulting, trends 110° (bisector of sets (1) and (2) trends). If displacements on sets (2) and (3) faults are negligible, then an estimated 10 km dextral shear across *ca* 7.5 km implies that the compressive axis trends 112°, and the ratio of the principal dimensions of the horizontal finite strain ellipse is 3.5. F_2 folding implies a shortening direction of 110° ± 20°, and thrust motions imply a shortening direction of *ca* 130°. Thus, the azimuth of the principal compressive axis and the ratio of the principal dimensions of the average horizontal finite strain ellipse lie within the stippled region on the graph in Fig. 17. Figure 17 also shows the variation with time, for 1 Ma increments, of both the aspect ratio of the horizontal finite strain ellipse and azimuth of the principal compressive axis, calculated using a range of constant velocity gradients of permanent deformation (Table 4, McKenzie & Jackson 1983). These suggest that the estimated finite deformation, as a consequence of D_2 deformation, could have been achieved in much less than 4 Ma.

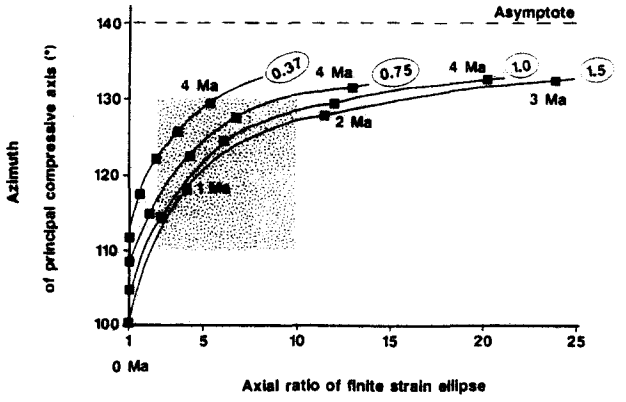

Fig. 17. Graph showing the variation in the aspect ratio of the horizontal strain ellipse and the azimuth of the principal horizontal compressive axis for 1 Ma time increments, marked by solid squares, and a range of constant velocity gradients. The azimuth is calculated from the shear zone model, discussed in the text, and approaches the asymptote (normal to trend of shear zone margin) after infinite deformation. The $\partial v/\partial y$ velocity gradient is the same in all cases (0.25×10^{-6} a^{-1}). The $\partial u/\partial y$ velocity gradient is ringed (units of 10^{-6} a^{-1}). The stippled region shows the estimated field of the azimuth of the compressive axis and the axial ratio for the average horizontal D_2 strain in the study area. This suggests that all the observed D_2 deformation could have occurred in much less than 4 Ma.

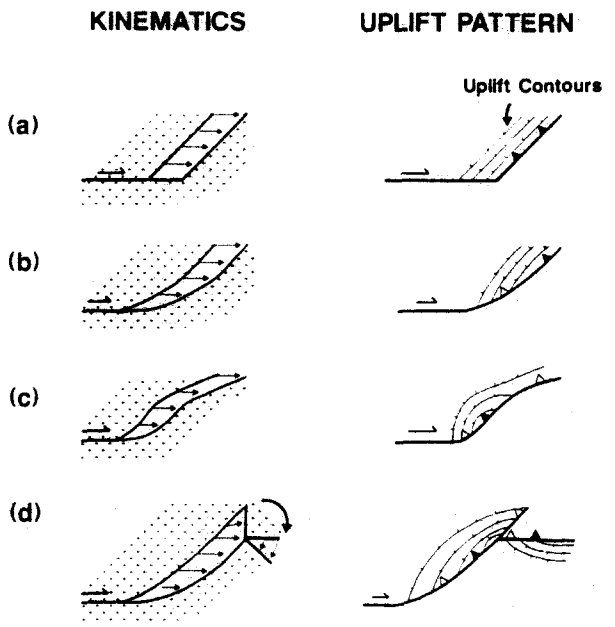

Fig. 18. Cartoons illustrating hypothetical relations between uplift and fault kinematics, if the uplift pattern reflects shortening across faults. Diagrams represent map views of faults with variable trends. The left-hand diagrams illustrate the relative motion of two fault blocks (ornamented with cross pattern), while the right-hand diagrams illustrate hypothetical uplift patterns, shown as contours of increasing uplift (ticks on down-hill side): (a) a sharp change in fault trend; (b) progressive change in trend; (c) two progressive changes in trend; (d) progressive change in trend and rotation of fault block at one end. Compare these with the uplift pattern in the Marlborough domains, shown in Fig. 14.

REGIONAL D_2 DEFORMATION

Translation kinematics

The dextral strike-slip rates on the major faults in the Marlborough domains vary between 4 and 15 mm a^{-1} (Berryman 1979, Kieckhefer 1979, Wellman 1983, Grapes & Wellman 1986). The summit heights are markedly higher on the NW side of the major NW-dipping faults in the northern Marlborough domain, suggesting a significant component of thrusting, though heights also vary along the length of the faults (Fig. 14, Kieckhefer 1979, Wellman 1983). The major ENE-trending fault planes in the southern Marlborough domain are subvertical and the uplift pattern suggests that, except for the Hope fault, the faults have a small vertical throw (Fig. 14) (Berryman 1979, Kieckhefer 1979, Wellman 1979, 1983). Fault-plane solutions from the southern Marlborough domain (Scholz *et al.* 1973, Arabasz & Robinson 1976) are dominantly strike-slip, with a mean slip vector trending *ca* 080° and subparallel to the major faults (Wellman 1983). All this suggests the transfer of motion from ENE-trending predominantly strike-slip faults in the southern Marlborough domain to *ca* NE-trending strike-slip faults with a significant component of thrusting in the northern Marlborough domain (Fig. 18a).

The increase in the summit heights towards the NE in the northern Marlborough domain, along the length of the Awatere and Clarence faults (Fig. 14), assuming the dips of the fault planes are constant, suggests an increase in the thrusting component towards the NE. This could be the result of a progressive swing in the trend of the faults from ENE in the southern Marlborough domain to NE in the northern Marlborough domain, with the greatest angular difference in trend coinciding with the region of maximum uplift (Figs. 14 and 18b). The decrease in differential uplift further NE may be a consequence of deformation between the major faults, resulting in tectonic rotation of fault blocks (Fig. 18d, see further on) and shortening elsewhere.

The region at the southwestern end of the Kekerengu fault, where it joins the Hope fault (Lensen 1962), is topographically high and may be being uplifted at rates as high as 10 mm a^{-1} (Fig. 14) (Wellman 1979). The strike-slip rate on the eastern end of the Hope fault is significantly less than further west (van Dissen 1987). Thus, a large proportion of the motion on the Hope fault is probably being transferred to the Kekerengu fault, accommodated by shortening and rapid uplift in an intervening transfer zone (Fig. 18c). Wellman (1983) has documented a north trending active thrust fault in this region. Domains H and I may form the eastern margin of the transfer zone, where ESE-shortening is occurring on N–NNE-trending folds and faults.

Rotation kinematics

Lamb (1988) has used the geodetic and fault slip data in the northern part of the South Island (Berryman 1979, Kieckhefer 1979, Bibby 1981, Wellman 1983, Walcott 1984a) to estimate the velocities of the regions between the major faults relative to the Pacific plate (Fig. 19).

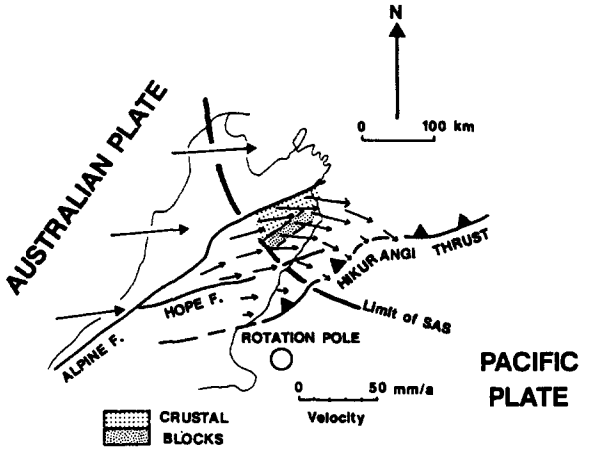

Fig. 19. Arrows represent estimates of the horizontal instantaneous velocities of the crust in the Marlborough fault system, relative to the Pacific plate. Large arrows show the velocities of the Australian plate relative to the Pacific plate, calculated from the instantaneous rotation pole and rate of Chase (1978). Other velocities were estimated from an integration of the available geodetic measurements and fault slip data (Lamb 1988). Velocity pattern suggests that large crustal blocks in the northern Marlborough domain are rotating clockwise at 8.5° ± 5.5° Ma^{-1} about poles located about 100 km south of the region. Heavy dashed line marks the southern edge of the underlying and seismically active subducted slab (SAS).

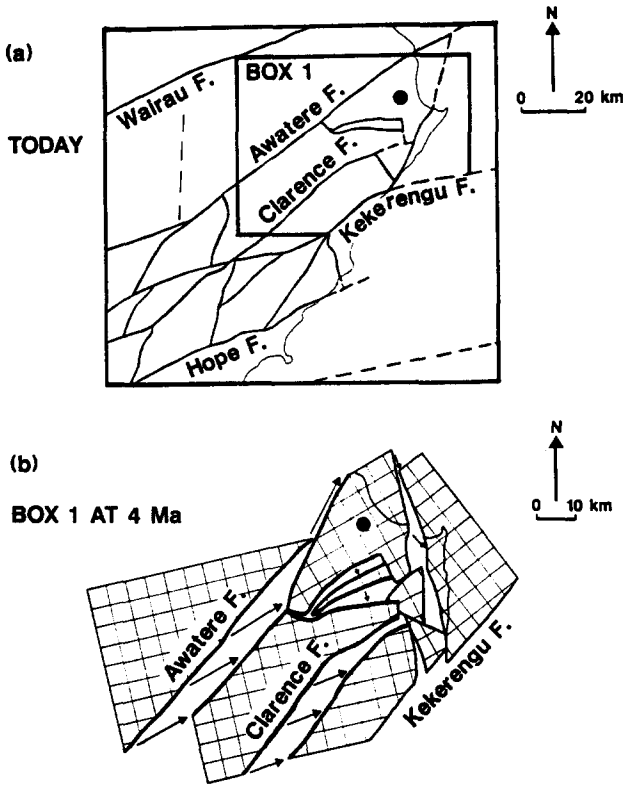

Fig. 20. Cut-out reconstruction of part of the northern Marlborough domain, based on the model of rotation suggested by the short-term velocities (Fig. 19), palaeomagnetism and estimates of the displacements on the major faults. (b) Postulated reconstruction at *ca* 4 Ma of the box 1 defined in (a). Grid pattern provides a reference for rigid body rotation, while blank regions between cut-out blocks represent the amount of shortening that has occurred across the major faults. Heavy lines in (b) represent block margins which have been reconstructed with some confidence. Other boundaries are speculative. A clockwise rotation about a vertical axis of *ca* 35° relative to True North in the last 5 Ma (Roberts 1986) has been determined palaeomagnetically at the locality marked by a black dot.

The velocities suggest that large elongate crustal blocks in the northern Marlborough domain, defined by the obvious lack of deformation in a Cretaceous volcanic complex and late Miocene cover sequences (Lamb 1988), are rotating clockwise relative to the Pacific plate at 8.5 ± 5.5° Ma^{-1}about poles located about 100 km south of Kaikoura (Fig. 19).

Palaeomagnetic measurements in Pliocene sediments located north of the study area (Fig. 2a) suggest a clockwise rotation about a vertical axis of *ca* 35° relative to True North (Roberts 1986). The gentle dips (<25°) and simple stratigraphy (Lensen 1962, Kennett 1966) in this region suggest that the rotation applies to a crustal block *ca* 30 × 30 km across between the Awatere and Clarence faults, bounded to the south by an E-trending thrust zone (King 1934) (Fig. 20a). A cut-out block reconstruction shows that a *ca* 15° clockwise rotation of this region, relative to further south (Fig. 20b), would require about 8 km of N–S shortening at the eastern end of the thrust zone. Mapping in this area (King 1934, Melhuish 1988) suggests that the shortening is not larger than this. Thus, at least 20° of the observed 35° of clockwise rotation may be of regional significance, representing the clockwise rotation of large elongate crustal blocks between the major faults in the northern Marlborough domain (Lamb 1988), including the major strike-slip faults, consistent with that inferred from the short-term deformation (Fig. 20b).

The estimated 20° of regional rotation during the last 4 Ma may have occurred in the study area, in addition to the local rotation, resulting in 50–60° of clockwise rotation about a vertical axis relative to the Pacific plate in Domain E since the early Pliocene.

Rotation and translation kinematics

The full kinematics of the Marlborough domains involves translation and rotation. Figure 21 shows a possible model where several large elongate crustal blocks (blocks A and B) in the northern Marlborough domain both rotate clockwise about vertical axes relative to the faults in the southern Marlborough domain, and also accommodate the dextral shear in the southern Marlborough domain. Dextral shear in the southern Marlborough domain may occur as both slip on the major faults and deformation, with vertical vorticity W', between the faults. The latter may involve rotation about vertical axes of small crustal blocks, similar to that in the McKenzie & Jackson (1983) trellis model (Fig. 21), with rotation rates equal to W'. Alternatively, small crustal blocks may be floating and rotating at rates generally less than W' ($W'/2$ if blocks are equidimensional), on a continuously deforming and underlying lithosphere (McKenzie & Jackson 1983, Lamb 1987). The boundary between the two domains is a series of hinges about which the major fault blocks in the northern

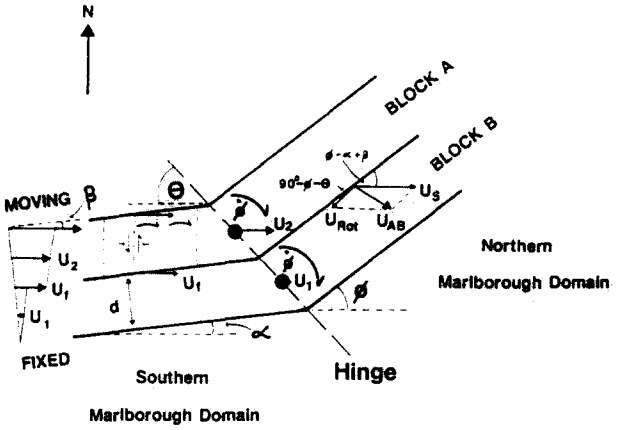

Fig. 21. Diagram illustrating a model for the rotation kinematics of the Marlborough domains, suggested by the instantaneous velocity and uplift pattern, as well as the palaeomagnetic data. The southern Marlborough domain may form a zone of predominantly dextral simple shear with a constant orientation, though with possibly internal rotation about vertical axes of small crustal blocks. This may be linked to large pivoting crustal blocks (blocks A and B) in the northern Marlborough domain which are separated by major faults (e.g. between blocks A and B). Slip on the major faults in the northern Marlborough domain accommodates both the rotation of the large crustal blocks (rotating at a rate $\dot{\phi}$ relative to True North), and also the dextral motions in the southern Marlborough domain. In the southern Marlborough domain, W is the average vertical vorticity vector, W' is the vertical vorticity of deformation between the major faults and d equals the spacing of the major faults. U_f is the slip vector a major fault in the southern Marlborough domain. U_{AB} is the velocity of block A relative to block B, and can be considered as a combination of U_{rot} as a consequence of the rotation of blocks A and B, and U_S, which is the velocity of the hinge of block A relative to the hinge of block B. Thus, assuming no velocity gradients parallel to the major faults in the southern Marlborough domain $U_2 - U_1 = U_f + W'd/\cos\beta = U_s = Wd/\cos\beta$, $U_{rot} = (d\dot{\phi})/\sin(\theta + \alpha)$. In the Marlborough domains, α is *ca* 20°, β is *ca* 15°, θ is *ca* 45°, ϕ is *ca* 35°.

Marlborough domain rotate. However, the hinges translate relative to the Pacific plate. The model implies that the angle between the major faults in the southern and northern Marlborough domains has changed with time.

The fault slip data (Berryman 1979, Kieckhefer 1979, Wellman 1983, Grapes & Wellman 1986) suggest that *ca* 70% of the relative plate motion in the northern part of the South Island is taken up by slip on the major faults. Therefore, the vertical vorticity of deformation (W') between the major faults in the southern Marlborough domain may be *ca* 0.3 times the average vertical vorticity (W) in this part of the plate-boundary zone. Taking $W = 4 \times 10^{-7}$ a^{-1} (50 mm a^{-1} across 120 km), then W' equals 1.2×10^{-7} a^{-1}. The rotation rate of the large crustal blocks (blocks A and B in Fig. 21) in the northern Marlborough domain, inferred from palaeomagnetismn to be *ca* 10^{-7} rads a^{-1}, is in the range $W'/2$ to W'. In addition, using values for the angles and dimensions in Fig. 21 appropriate to the Marlborough domains, the model suggests that the dextral strike-slip rate on the major faults in the northern Marlborough domain is presently *ca* 0.7 times that on the major faults in the southwestern Marlborough domain, which is compatible with available slip rate data.

DEVELOPMENT OF THE PLATE-BOUNDARY ZONE

Ocean floor magnetic anomalies suggest that the relative motion between the Pacific and Australian plates commenced between 45 and 35 Ma (Stock & Molnar 1982), resulting in the subduction of the Pacific plate in the northern part of the New Zealand plate-boundary zone. Moreover, the structural and sedimentary history suggests that the position of the plate-boundary zone changed with time.

Changes in the plate margin

The Chatham Rise on the Pacific plate (Figs. 1a and 22c) intersects the southern end of the Hikurangi subduction zone and marks a passive boundary between continental- and oceanic-type crust. A plate reconstruction for the Lower Tertiary, at the inception of the plate-boundary zone in New Zealand (Stock & Molnar 1982, Walcott 1987), shows that the Chatham Rise approximately lined up with the continental margin on the Australian plate, along the NE edge of the Auckland Peninsula (Fig. 1a), with the Hikurangi margin bridging the intervening zone. Subsequently, continental crust along part of this boundary overrode the subducted oceanic-type crust (Fig. 22a). It follows that the southern edge of the unfolded subducted slab should mark the initial orientation of both the original continental–oceanic crust boundary and trench in this part of the plate-boundary zone (Walcott 1979). The southern limit of the unfolded seismically active subducted slab trends NW (Figs. 16 and 22c) (Ansell & Adams 1986), but some

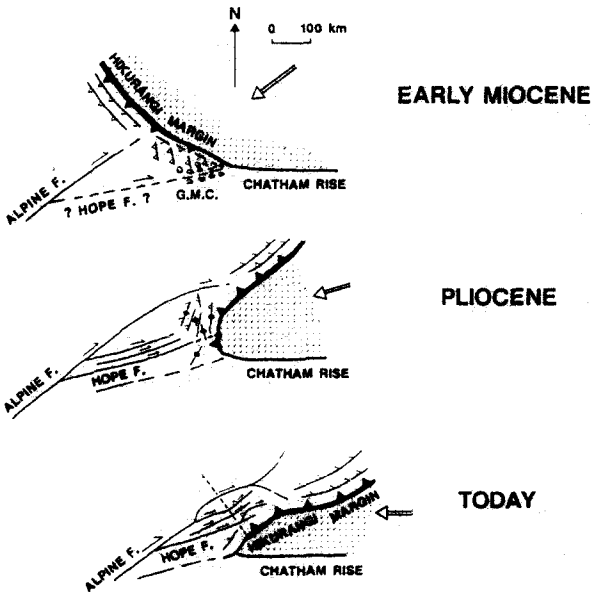

Fig. 22. Cartoon maps illustrating the possible structural evolution in the Marlborough region. It is suggested that this region has formed a hinge at the southern end of the Hikurangi margin as the margin swung round from a W–NW trend in the early Miocene to a NE trend today. Large arrow shows the relative plate vector for each period. Ornamented region represents subductable thin Pacific plate crust, which is juxtaposed with continental crust along the Chatham Rise.

of the slab may be aseismic. Plate reconstructions based on ocean floor magnetic anomalies (Walcott 1987) suggest that the W-trending projection of the northern margin of the Chatham Rise was the initial position of the trench. In this case, a large triangular region of currently aseismic subducted slab underlies the southern Marlborough domain.

A scissor-type subduction, hinged in the Marlborough domains, resulted in the margin of the overriding Australian plate (Hikurangi margin) swinging round from a W to NW trend (Fig. 22a) to the present NE trend (Fig. 22c, Walcott 1979, 1984b, 1987). Paleomagnetic rotation data provides independent evidence for the progressive clockwise rotation of crustal blocks in the overriding Australian plate (Walcott *et al.* 1981, Walcott & Mumme 1982, Mumme & Walcott 1985). Thus, the structural history in the northern Marlborough domain suggests that the hinge initially formed a thrust belt (D_1 deformation) in the Miocene, coeval with the deposition of a submarine fan complex (Fig. 22a), and became a dextral shear zone (D_2 deformation) in the Plio-Pleistocene (Figs. 22b & c).

Miocene deformation (D_1)

The direction of relative plate motion in the Marlborough domains in the early Miocene trended *ca* SW (Fig. 22a) (Smith 1981). This trend was at a high angle to the inferred initial trend of the plate margin and trench (W–NW). The geometry of the D_1 thrust complex is not well understood. However, D_1 thrusts in Domain A cut up-section towards the E and SE (cross-section AA'A" in Fig. 4) (Prebble 1976). Near the Clarence fault, they dip steeply and strike parallel to the Clarence fault plane, suggesting that part of the Clarence fault may be a reactivated and steepened D_1 thrust. Further north, major D_2 structures have a more northerly trend and may also have reactivated older D_1 structures. Thus, a reconstruction of the northern Marlborough domain in the early Miocene, taking into account D_2 deformation and tectonic rotation, suggests a complex zone of NNW- and WNW-trending thrusts, at a high angle to the direction of relative plate motion at that time (Fig. 22a).

It is not clear whether the major strike-slip faults in southern Marlborough domain were active in the early Miocene. At the rates of D_2 deformation, the likely strike-slip offsets on these faults (Lensen 1962, this study) could have been achieved in the last 4 Ma. Rotation of the Hikurangi margin in the Miocene may therefore have been accommodated by thrusting in the northern Marlborough domain, with an increase in the shortening across these thrusts towards the W or NW at that time. The southern limit of the Great Marlborough Conglomerate may have marked the Pacific plate boundary (Fig. 22a).

Plio-Pleistocene deformation (D_2)

Changes in the relative plate motion resulted in a substantial compressional component on the Alpine fault by the early Pliocene, with the development of the Southern Alps (Fig. 1b) and the D_2 deformation in the northern Marlborough domain. A reconstruction at this time (Fig. 22b) suggests that a *ca* 100 km long segment of Hikurangi margin in the Marlborough region trended approximately north. D_2 appears to have initiated as en échelon N- to NE-trending km-scale F_2 folds, which may have nucleated on pre-existing D_1 structures. Continued folding resulted in the steepening of the D_1 structures, which were reactivated as steep reverse dextral strike-slip faults.

There is no evidence for deformation between the Pacific plate and the major dextral faults in the southern Marlborough domain which could have accommodated significant clockwise rotation (>10°) about vertical axes of these faults relative to the Pacific plate. Indeed, several published reconstructions of the Marlborough fault system suggest that the faults have rotated *ca* 15° *anticlockwise* (Merzer & Freund 1974, Norris 1979, Garfunkel & Ron 1985). Thus, in the Pliocene, an E- to ENE-trending dextral shear zone in the southern Marlborough domain may have connected with N- to NNE-trending thrust faults in the northern Marlborough domain (Fig. 22c). Progressive rotation of the plate margin involved rotation of the thrust faults in the northern Marlborough domain, with an increase in the strike-slip component on these faults, bringing them into closer alignment with the faults in the southern Marlborough domain and also the direction of relative plate motion.

CONCLUSIONS

This paper has described a complex structural history which has accommodated a drastic rotation of the trend of the subduction zone between the Australian and Pacific plates. The structural history has been derived from an analysis of many aspects of the deformation, such as geodetic deformation, seismicity, uplift data, palaeomagnetic rotations, detailed structural mapping, combined with an understanding of the stratigraphy and relative plate motions. Deformation commenced in the latest Oligocene or early Miocene with the development of a thrust belt oriented at a high angle to the vector of relative plate motion at that time. Subsequent deformation, involving the rotation about vertical and horizontal axes of the early thrusts, accommodated a clockwise rotation of the trend of the subduction zone. Since the Pliocene, deformation has been dominated by dextral shear, involving major strike-slip faults and localized zones of distributed deformation. The amount and complexity of deformation, especially during the last 4 Ma, serves to emphasize the difficulties in unscrambling ancient deformed zones, where the age and plate-tectonic setting are not well known.

Acknowledgements—This work was carried out while S. H. Lamb held a 3 year New Zealand University Grants Committee post-doctoral fellowship at Victoria University of Wellington, New Zealand.

REFERENCES

Ansell, J. & Adams, D. 1986. Unfolding the Wadati-Benioff zone in the Kermadec–New Zealand region. *Phys. Earth & Planet. Interiors* **44**, 274–280.

Arabasz, W. J. & Robinson, R. 1976. Microseismicity and geologic structure in the northern South Island, New Zealand. *N.Z. Jl Geol. Geophys.* **19**, 569–601.

Berryman, K. 1979. Active faulting and derived PHS directions in the South Island, New Zealand. In: *The Origin of the Southern Alps* (edited by Walcott, R. I. & Cresswell, M. M.). *Bull. R. Soc. N.Z.* **18**.

Bibby, H. M. 1981. Geodetically determined strain across the southern end of the Tonga–Kermadec–Hikurangi subduction zone. *Geophys. J. R. astr. Soc.* **66**, 513–533.

Browne, G. H. & Field, B. D. 1985. The lithostratigraphy of Late Cretaceous to Early Pleistocene rocks of northern Canterbury, New Zealand. *N.Z. geol. Surv. Rec. 6.*

Chappell, J. 1974. Geology of coral terraces, Huon Peninsula, New Guinea: a study of Quaternary tectonic movements and sea-level changes. *Bull. geol. Soc. Am.* **85**, 553–570.

Chase, C. G. 1978. Plate kinematics: the Americas, East Africa and the rest of the world. *Earth Planet. Sci. Lett.* **37**, 353–368.

Garfunkel, Z. & Ron, H. 1985. Block rotation and deformation by strike-slip faults 2. The properties of a type of macroscopic discontinuous deformation. *J. geophys. Res.* **90**, 8589–8602.

Ghani, M. A. 1974. Late Cenozoic vertical crustal movements in the central part of New Zealand. Unpublished Ph.D. thesis, Victoria University, Wellington, New Zealand.

Ghani, M. A. 1978. Late Cenozoic vertical crustal movements in the central part of New Zealand. *N.Z. Jl Geol. Geophys.* **21**, 117–125.

Grapes, R. H. & Wellman, H. W. 1986. The north-east end of the Wairau Fault, Marlborough, New Zealand. *J. R. Soc. N.Z.* **16**, 245–250.

Kennett, J. P. 1966. Faunal Succession in Two Upper Miocene–Lower Pliocene Sections, Marlborough, New Zealand. *Trans. R. Soc. N.Z. Geol.* **3**, 197–213.

Kieckhefer, R. M. 1979. Sheets M31D, N31A, N31C, and parts of M32A and M32B Leader Dale (1st edn), Sheets N31B and N31D Dillon (1st edn) Late Quaternary Tectonic Map of New Zealand 1:50,000. Department of Scientific and Industrial Research, Wellington, New Zealand.

King, L. C. 1934. The geology of the lower Awatere district, Marlborough. *Mem. N.Z. geol. Surv.* **2**.

Lamb, S. H. 1987. A model for tectonic rotations about a vertical axis. *Earth Planet. Sci. Lett.* **84**, 75–86.

Lamb, S. H. 1988. Tectonic rotations about vertical axes during the last 4 Ma in part of the New Zealand plate-boundary zone. *J. Struct. Geol.*, **10**, 875–893.

Lamb, S. H. & Vella, P. 1987. The last million years of deformation in part of the New Zealand plate-boundary zone. *J. Struct. Geol.* **9**, 877–891.

Lensen, G. J. 1962. Sheet 16, Kaikoura (1st Edn). Geological Map of New Zealand 1:250,000. Department of Scientific and Industrial Research, Wellington, New Zealand.

Lewis, K. B. (editor) 1985. *New Seismic Profiles, Cores and Dated Rocks from the Hikurangi Margin, New Zealand. N.Z. Oceanogr. Inst. Field Rep.* **22**.

McFadgen, B. G. 1987. Beach ridges, breakers and bones: late Holocene geology and archaeology of the Fyffe site, S49/46, Kaikoura Peninsula, New Zealand. *J. R. Soc. N.Z.* **17**, 381–394.

McKenzie, D. P. & Jackson, J. A. 1983. The relationship between strain rates, crustal thickening, palaeomagnetism, finite strain and fault movements within a deforming zone. *Earth Planet. Sci. Lett.* **65**, 182–202.

Melhuish, A. 1988. Geology of Colonel Gully and adjacent regions, upper Awatere valley, Marlborough, New Zealand. Unpublished B.Sc. (Hons) dissertation, Victoria University, Wellington, New Zealand.

Merzer, A. M. & Freund, R. 1974. Transcurrent Faults, Beam Theory and the Marlborough Fault System, New Zealand. *Geophys. J. R. astr. Soc.* **38**, 553–562.

Mesollela, K. R., Mathews, R. K., Broecker, W. S. & Thurber, D. L. 1969. The astronomical theory of climatic change: Barbados data. *J. Geol.* **77**, 250–274.

Mumme, T. C. & Walcott, R. I. 1985. Palaeomagnetic studies at Geophysics Division 1980–1983. Department of Scientific and Industrial Research, Geophysics Division Report 204.

New Zealand Geological Survey, 1972. North Island and South Island (1st edn), Geological map of New Zealand 1:1,000,000. Department of Scientific and Industrial Research, Wellington, New Zealand.

Norris, R. J. 1979. A geometrical study of finite strain and bending in the South Island, New Zealand. In: *The Origin of the Southern Alps* (edited by Walcott, R. I. & Cresswell, M. M.). *Bull. R. Soc. N.Z.* **18**.

Osborne, 1980. Geology of the Clarence-Kekerengu sector, Marlborough, South Island, New Zealand. Unpublished M.Sc. thesis, University of Canterbury, Christchurch, New Zealand.

Prebble, W. M. 1976. Geology of Kekerengu–Waima River, Marlborough, New Zealand. Unpublished M.Sc. thesis, Victoria University of Wellington, New Zealand.

Roberts, A. P. 1986. Palaeomagnetic study of the Blind River Section, Marlborough, South Island, New Zealand. Unpublished B.Sc. (Hons) dissertation, Victoria University, Wellington.

Robinson, R. 1986. Seismicity, structure, and tectonics of the Wellington region, New Zealand. *Geophys. J. R. astr. Soc.* **87**, 379–409.

Scholz, C. H., Rynn, J. M. W., Weed, R. W. & Frohlich, C. 1973. Detailed seismicity of the Alpine Fault Zone and Fiordland Region, New Zealand. *Bull. geol. Soc. Am.* **84**, 3297–3316.

Smith, E. G. C. 1981. Calculation of poles of instantaneous rotation from poles of finite rotation. *Geophys. J. R. astr. Soc.* **65**, 223–227.

Stock, J. & Molnar, P. 1982. Uncertainties in the relative positions of the Australia, Antarctica, Lord Howe and Pacific Plates since the Late Cretaceous. *J. geophys. Res.* **87**, 4679–4714.

Suggate, R. P., Stevens, G. R. & Te Punga, M. T. (editors) 1978. *The Geology of New Zealand.* Government Printer, Wellington, New Zealand.

van Dissen, R. J. 1987. Late Quaternary faulting in the Kaikoura region, southeastern Marlborough, New Zealand. Abstracts of the Annual Conference of the New Zealand Geological Society, Dunedin.

Walcott, R. I. 1978. Present tectonics and Late Cainozoic evolution of New Zealand. *Geophys. J. R. astr. Soc.* **52**, 137–164.

Walcott, R. I. 1979. Plate motion and shear strain rate in the vicinity of the Southern Alps. In: *The Origin of the Southern Alps* (edited by Walcott, R. I. & Cresswell, M. M.). *Bull. R. Soc. N.Z.* **18**.

Walcott, R. I. 1984a. The kinematics of the plate-boundary zone through New Zealand: a comparison of short- and long-term deformation. *Geophys. J. R. astr. Soc.* **79**, 613–633.

Walcott, R. I. 1984b. Reconstructions of the New Zealand region for the Neogene. *Palaeogeogr. Palaeoclimatol., Palaeoecol.* **46**, 217–231.

Walcott, R. I. 1987. Geodetic strain and the deformational history of New Zealand during the late Cainozoic. *Phil. Trans. R. Soc. Lond.* **A321**, 163–181.

Walcott, R. I., Christoffel, D. A. & Mumme, T. C. 1981. Bending within the axial tectonic belt of New Zealand in the last 9 Ma from palaeomagnetic data. *Earth Planet. Sci. Lett.* **52**, 427–434.

Walcott, R. I. & Mumme, T. C. 1982. Palaeomagnetic study of the Tertiary sedimentary rocks from the East Coast of the North Island, New Zealand. Department of Scientific and Industrial Research, Geophysics Division Report 189.

Wellman, H. W. 1948. Tararua Range summit height accordance. *N.Z. J. Sci. Technol.* **30B**, 123–127.

Wellman, H. W. 1979. An uplift map for the South Island of New Zealand, and a model for uplift of the Southern Alps. In: *The Origin of the Southern Alps* (edited by Walcott, R. I. & Cresswell, M. M.). *Bull. R. Soc. N.Z.* **18**.

Wellman, H. W. 1983. New Zealand horizontal kinematics. In: *Geodynamics of the Western Pacific–Indonesian Region* (edited by Hilde, T. W. C. & Uyeda, S.). *Am. Geophys. Un. Geodynamic Series*, **11**, 4523–457.

Woodcock, N. H. 1986. The role of strike-slip fault systems at plate boundaries. *Phil. Trans. R. Soc. Lond.* **A317**, 13–29.